NEANDC (E) - 172 U Vol.5
INDC (Ger) - 18/L + Special

PROGRESS REPORT ON NUCLEAR DATA RESEARCH IN THE FEDERAL REPUBLIC OF GERMANY

for the Period January 1 to December 31, 1975

July 1976

Editor:
S. W. Cierjacks
Institut für Angewandte Kernphysik
Kernforschungszentrum Karlsruhe

NEANDC (E) - 172 U Vol.5
INDC (Ger) - 18/L + Special

PROGRESS REPORT
ON NUCLEAR DATA RESEARCH IN THE FEDERAL REPUBLIC OF GERMANY

for the Period January 1 to December 31, 1975

July 1976

Editor:
S. W. Cierjacks
Institut für Angewandte Kernphysik
Kernforschungszentrum Karlsruhe

P R E F A C E

This report is prepared for nuclear data research information exchange among member states of IAEA and NEA. It brings together reports from the GfK Karlsruhe, the KFA Jülich, the GKSS Geesthacht, the EIT Karlsruhe, the Universities of Hamburg, Mainz and Munich and from the ZAED Karlsruhe. The publication of this report was supported by the Fast Breeder Project of the Karlsruhe Research Centre.

All contributions are presented under a laboratory heading. Where the work is relevant to requests in the World Request List for Nuclear Data Measurements, WRENDA 74 (INDC(SEC)-38U) the corresponding request numbers are listed after the titles and the authors' names of the contributions.

CONTENTS

INSTITUT FÜR ANGEWANDTE KERNPHYSIK II
KERNFORSCHUNGSZENTRUM KARLSRUHE

1. Isochronous Cyclotron

1.1 γ-Ray Production Cross Sections of Structural Materials

F. Voß, S. Cierjacks, D. Erbe, G. Schmalz
(Relevant to request numbers: 661012, 732040, 661024, 712008)

Previous studies on neutron induced γ-ray production cross sections of structureal materials were continued with the investigations of low lying γ-ray transitions in some chromium and nickel isotopes. The experimental device was a slightly modified arrangement of the system described earlier (1). γ-rays produced in inelastic neutron scattering on the isotopes contained in the natural elements were measured at a back-angle of 125^{o}. At this position the Legendre polynomial P_2 is zero, so that - for most of the strong transitions observed in the experiment - the total γ-ray production cross section can be obtained by multiplication of the measured differential cross section with 4π. In the new investigations the following transitions were studied: The 781 keV γ-line in ^{50}Cr, the 935, 1332, 1434, 1531, 1728 keV γ-lines in ^{52}Cr; the 1005 and 1454 keV γ-line in ^{58}Ni and the 467, 826, 1173, 1333 keV γ-lines in ^{60}Ni. Excitation functions for the production of the respective γ-lines were measured by time-of-flight from threshold to 10 MeV with an energy resolution of the incident neutrons ranging from 2.2 keV at 1 MeV to 70 keV at 10 MeV. Preliminary results of the experiments were presented at the 1975 Washington Conference on Nuclear Cross Sections and Technology. A typical result of this work is shown in Fig. 1. In this illustration the present results are compared with compiled results from other laboratories (2-4).

1.2 Inelastic Neutron Scattering on ^{238}U

F. Voß, S. Cierjacks
(Relevant to request numbers: 692387, 692393, 742083, 691270, 692391, 702030, 714018

In 1975 an analysis of our previous measurements of the γ-ray production cross sections from inelastic neutron scattering on ^{238}U was performed. First results of the excitation functions between thresholds and 5.5 MeV were obtained for transitions to the following ^{238}U final states: 680,

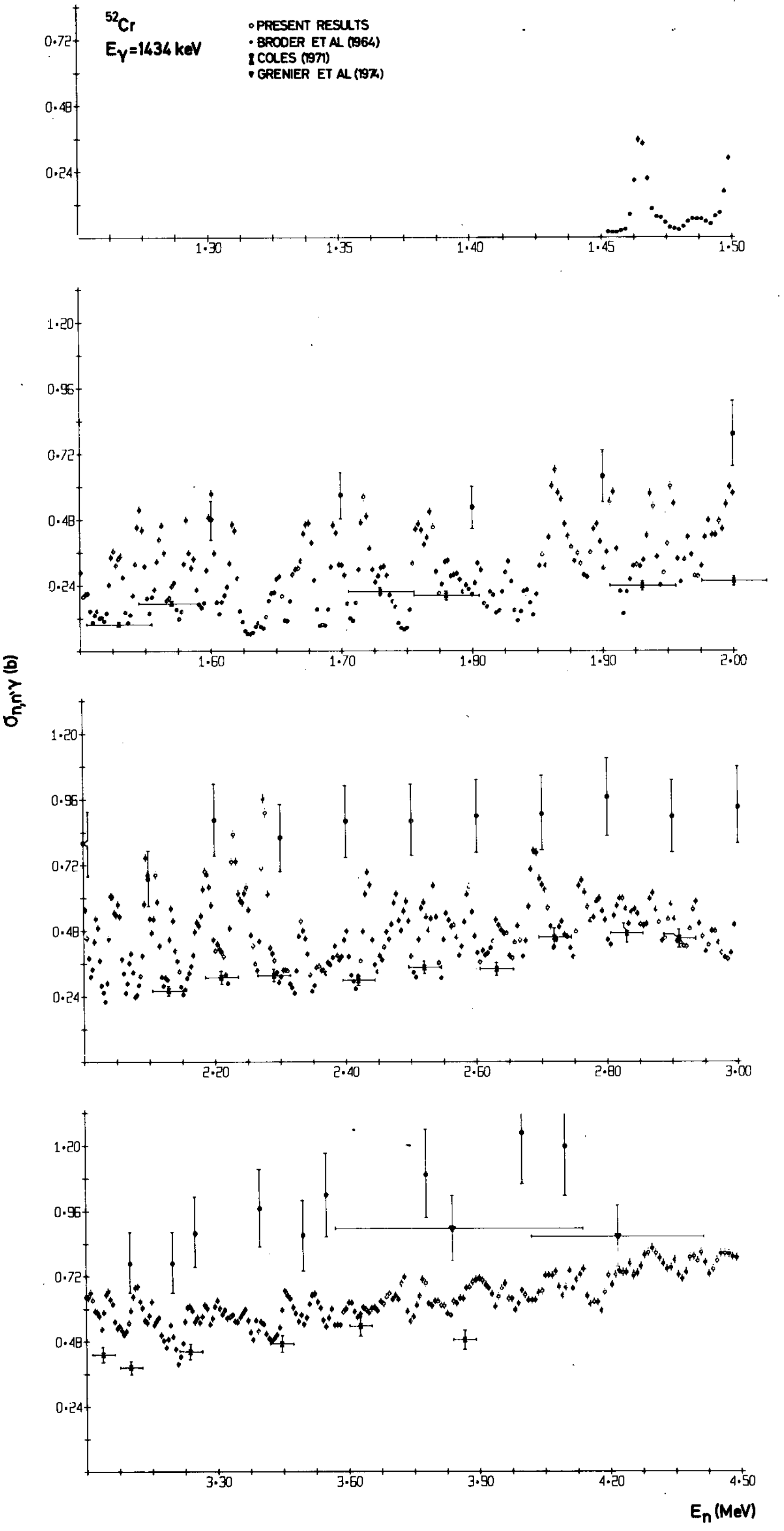

Fig. 1 Cross Section for the production of the 1434 keV γ line of ^{52}Cr from inelastic neutron scattering

731, 927 + 931, 997, 1060 and 1061 keV. The remarkable feature was, that between threshold and about 2 MeV the present data are for several inelastic channels significantly lower (up to 30 %) than those from other laboratories employing neutron counting. The deviation of our data from previous results is in qualitative agreement with new integral measurements (5).

1.3 Elastic Neutron Scattering on ^{16}O and ^{28}Si

I. Schouky, S. Cierjacks
(Relevant to request numbers: 661028, 691115, 691116, 692021, 692022, 712004)

In the process of performing evaluations for shielding purposes, it was previously noted, that large deficiencies of elastic scattering cross sections existed for various shielding materials at several energy intervals between $\sim$1 and 10 MeV. In order to provide the lacking cross sections in the deficient regions and improved high-resolution data elsewhere, we have determined the elastic scattering cross sections of O and Si between 0.5-6 MeV at 10 scattering angles with high resolution using the fast neutron time-of-flight spectrometer. From the large number of the totally available results, Figs. 2-3 show two characteristic examples of the O data between 1.2 and 2.6 MeV and of the Si data between 1.2 and 2.6 MeV. The upper three curves are the differential elastic scattering cross sections for three selected scattering angles, the bottom curves represent the high-resolution total neutron cross sections, measured in this laboratory previously. High-resolution measurements of the differential elastic scattering provided a sensitive method to unambiguously determine spins and parities of the closely spaced, but non-overlapping resonances. Thus, the l- and J-values of 34 levels in O between 0.5 and 6 MeV and of 24 levels in Si between 0.5 and 2 MeV could be assigned from a study of the resonance shapes as a function of the scattering angle. A list of spin and partiy assignments of oxygen resonances in the range from 0.5 to 6 MeV is given in Table I.

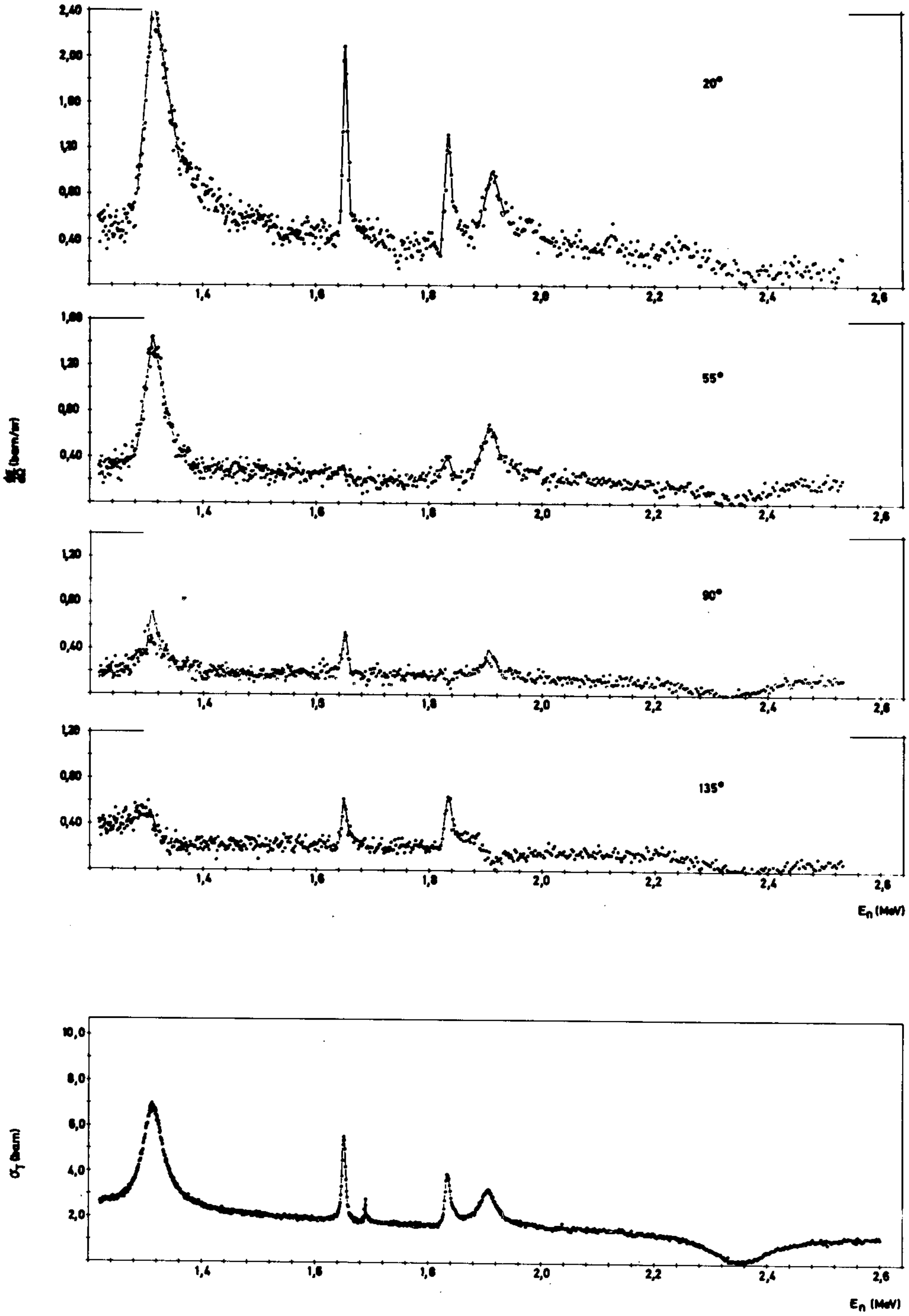

Fig. 2 Total and differential elastic scattering cross section of oxygen between 1.2 and 2.6 MeV

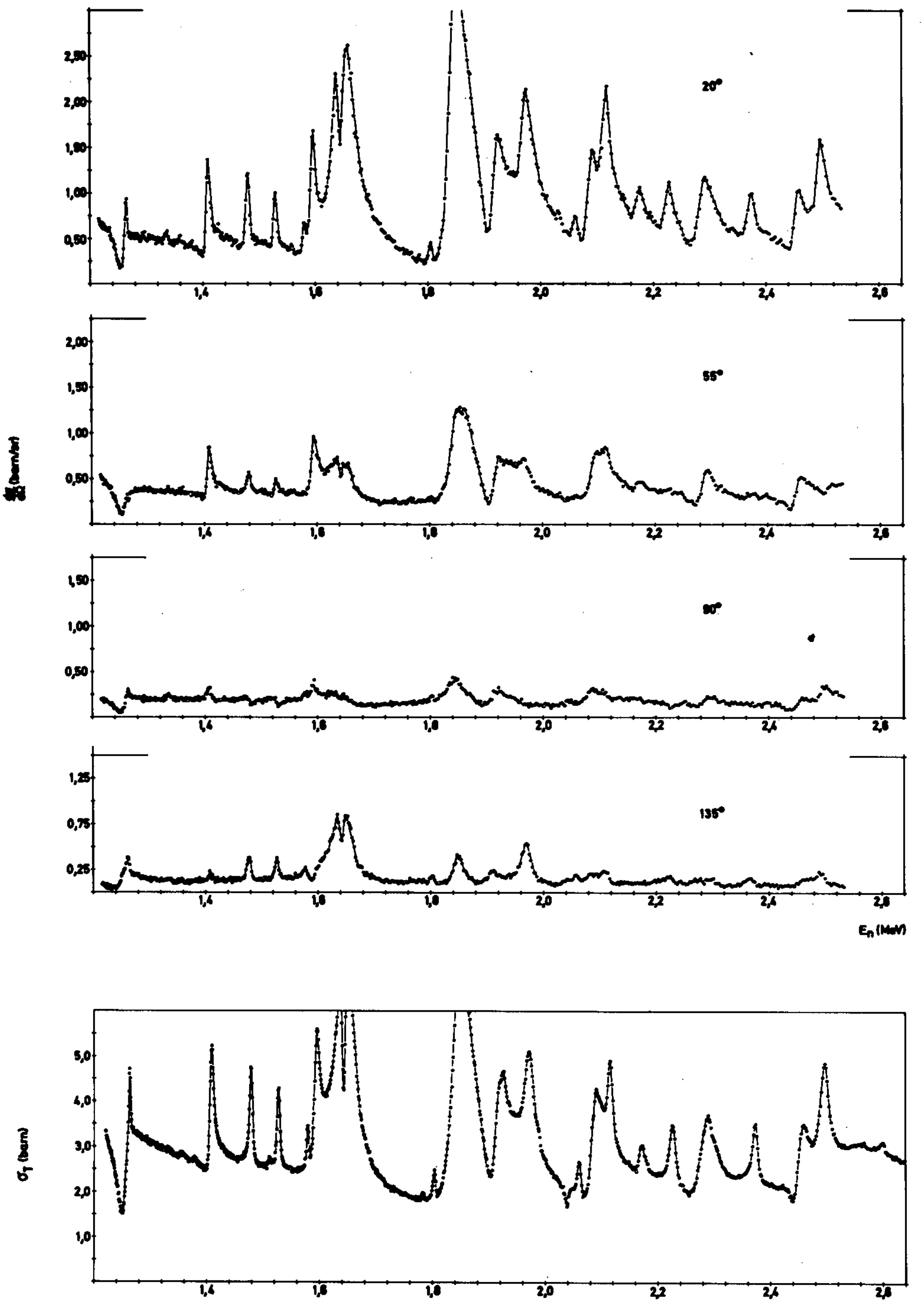

Fig. 3 Total and differential elastic scattering cross section of silicon between 1.2 and 2.6 MeV

Table 1: Spin and Parity Assignments for Neutron Resonances of $n + {}^{16}O$

E_n (MeV)	$E_{^{17}O}$ (MeV)	J^π	E_n (MeV)	$E_{^{17}O}$ (MeV)	J^π
1.009	5.083	$3/2^+$	4.162	8.060	$3/2^+$
1.303	5.377	$3/2^-$	4.29	8.18	$1/2^-$
1.651	5.696	$7/2^-$	4.31	8.197	$3/2^-$
1.689	5.731	$>1/2^+$	4.449	8.347	$1/2^+$
1.833	5.867	$3/2^+$	4.505	8.403	$5/2^+$
1.908	5.937	$1/2^-$	4.600	8.468	$7/2^+$
2.353	6.354	$1/2^+$	4.610	8.48	$\geq 3/2$
2.889	6.860	$1/2^-$	4.630	8.501	$5/2^-$
3.006	6.970	$1/2^-$	4.83	8.685	$3/2^-$
3.211	7.164	$5/2^-$	5.05	8.892	$3/2^+$
3.25	7.20	$3/2^+$	5.060	8.90	$7/2^-$
3.438	7.378	$5/2^+$	5.123	8.963	$7/2^-$
3.441	7.381	$5/2^-$	5.200	9.140	$1/2^-$
3.63	7.56	$3/2^-$	5.22	9.16	$9/2^-$
3.766	7.685	$7/2^-$	5.24	9.18	$7/2^-$
3.84	7.76	$11/2^-$	5.255	9.195	$5/2^+$
4.053	7.952	$1/2^+$	5.61	9.42	$3/2^-$
4.09	7.99	$1/2^-$	5.675	9.485	$5/2^-$

1.4 Analysis of s-Wave Resonances of ^{56}Fe between 450 and 850 keV+)

S. Cierjacks, G. Schmalz, R.R. Spencer, F. Voß

(Relevant to request numbers: 721038, 721041, 721042)

Fragmented intermediate doorway resonances of ^{56}Fe with spin and parity of $J = 1/2^{+}$ were predicted in previous theoretical investigations (6) near 400 and 750 keV. While the nature of the resonance at ∿400 keV could be well identified from detailed experimental studies of fine structure resonances, an unambiguous identification of the resonance at ∿ 750 keV was prohibited by the lack of sufficiently well resolved scattering data. In a recent transmission experiment at the cyclotron spectrometer with a resolution of 0.015 ns/m the resonance structure was mainly completely resolved, so that a resonance analysis became possible. From the highly resolved transmission data of two largely different sample thicknesses resonance parameters were determined by a multilevel R-matrix analysis. In Fig. 4 an R-matrix least-squares fit to both transmission curves simultaneously is shown. The analysis provided a unique determination of s-wave resonance parameters. The s-wave resonance parameters were used for a test of the sum rule for the reduced widths. The result is demonstrated in Fig. 4b which compares the summlation of the reduced widths of s-wave fine structure resonances with the width of the intermediate resonance. This figure shows a rather good agreement with a sum rule.

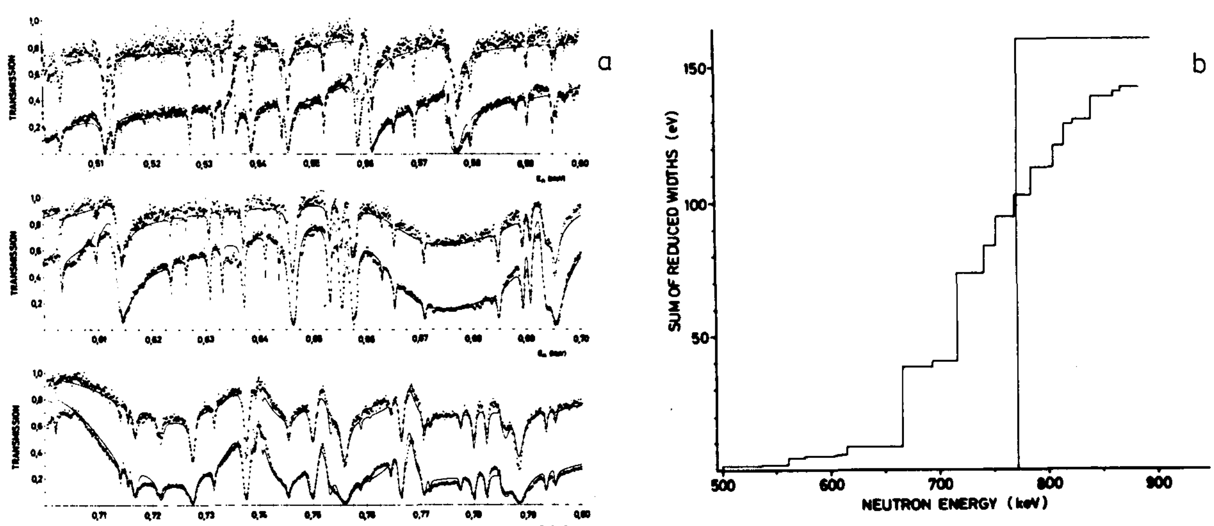

Fig. 4 a) Transmission of two different iron samples. The solid curve is a R-matrix multilevel fit.

b) Check of the sum rule for s-wave resonances between 500 and 850 keV

+) Work partly presented at the 1975 Washington Conference on Nuclear Cross Sections and Technology

1.5 Fast Fission Cross Sections of ^{239}Pu and ^{240}Pu

K. Kari, B. Leugers, S. Cierjacks

(Relevant to request numbers: 691467, 692426, 693070, 693071, 714024, 742006, 742099, 712086, 714030, 721088, 721091, 742009, 742022, 742105)

The measurements of the fission cross sections of ^{239}Pu and ^{240}Pu between 0.5 and 20 MeV were prepared for 1976. Up to now the existing gas scintillation device was modified towards a better compatibility for high counting rates and an improved discrimination against α-background. This was mainly achieved by optimizing the photomultiplier parameters of the scintillation counters and by modifying the electronic circuitry of the data aquisition system. Another problem was connected with the lifetimes of fission samples of large size. For large 7 cm diameter fission samples of hundred μgr layers, the thin vyns backings were damaged by α-recoil in an unacceptably short time. Preserving 4π detection the only practicable solution was to drastically reduce the sample diameters and the layer thicknesses. i.e. the amount of fissile materials, and to run the experiment at a short flight path. Measurements under these conditions are planned for early spring 1976.

1.6 Absolute Neutron Flux Measurements in Fast Neutron Spectra+)

I. Schouky, S. Cierjacks

A flux detector was developed in order to determine the fast neutron flux between 1 - 30 MeV obtained with the Karlsruhe isochronous cyclotron. The counter system represents a telescope-like proton recoil device using solid radiators and gas scintillation counters. Flux determination is accomplished separately between about 0.5 - 6 MeV and 5 - 30 MeV with a small interval of overlap. Below 6 MeV, recoil protons are detected in a single gas scintillation chamber viewed by three photomultipliers, requiring a fast coincidence. Above this range high energy recoil protons are identified by coincidences in three adjacent chambers arranged in series along the beam axis and by their specific energy losses. Since the transmission of the entire flux counting system in the whole energy region from 0.5 - 30 MeV is higher than 99 %, it can be used for simultaneous flux measurements in partical cross section experiments. The presently

---

+) Part of the work presented at the 1975 Washington Concerence on Nuclear Cross Sections and Technology achieved accuracy for the determination of the neutron flux is about 4 %.

1.7 Study of Fission Fragment Masses and Neutron Yields from the $^{233}U(d,pf)$ Reaction

S. Cierjacks, Y. Patin [+], J. Lachkar [+], J. Sigaud [+], C. Humeau [+], J. Chardin [++]

A measurement of fission fragment masses and neutron yields in $^{233}U(d,pf)$ reactions was performed at the Super EN tandem Van-de-Graaff accelerator of the Service de Physique Nucléaire at the Centre d'Etudes de Bruyères-le-Châtel (7). For a determination of the energies and the velocities of both fission fragments cooled silicon surface barrier detectors were employed. Time-of-flight measurements of fission products were accomplished by the associated particle method, using the protons emitted in the d,pf-reaction. In order to study also asymmetry effects in fission product emission, fragments were counted in two pairs of diodes placed at 0^o and 90^o relative to the ^{234}U recoil axis. The time resolution achieved with the surface barrier detectors operated at -100^oC was of the order of 0.2 ns. Assuming a time resolution of the same amount for the proton detector and taking into account the usual energy resolutions, it is expected that fragment masses can be determined with an uncertainty of $\sim \pm 3$ amu. This number is valid for a 15 cm flight path length chosen in the present experiment. The measured data covering about 10^6 counts will be evaluated off-line event by event. Conversion of analog and time-of-flight informations from the proton and the fission detectors provides the ^{234}U excitation energy and both fragment energies and masses before and after neutron emission and thus, the neutron yield as a function of the fission fragment mass. Resolutions obtained in the experiment measurements are demonstrated in Figs. 5 a,b. These illustrations show two-parametric contour plots for $(T_1 \times T_2)$ and $(E_1 \times E_2)$ of fission fragments detected at 0^o to the ^{234}U recoil axis. It can be seen that the fragments are well separated in both, the energy and the velocity representation, although the best separation is in the velocity spectrum. The off-line program for the evaluation of the raw data has mainly been set up and is in a first test stage. Its completion is expected for the next

---

[+] Service de Physique Nucléaire, Centre d'Etudes de Bruyères-le-Châtel few months, so that first results on mass distributions and neutron yields might be available in summer 1976.

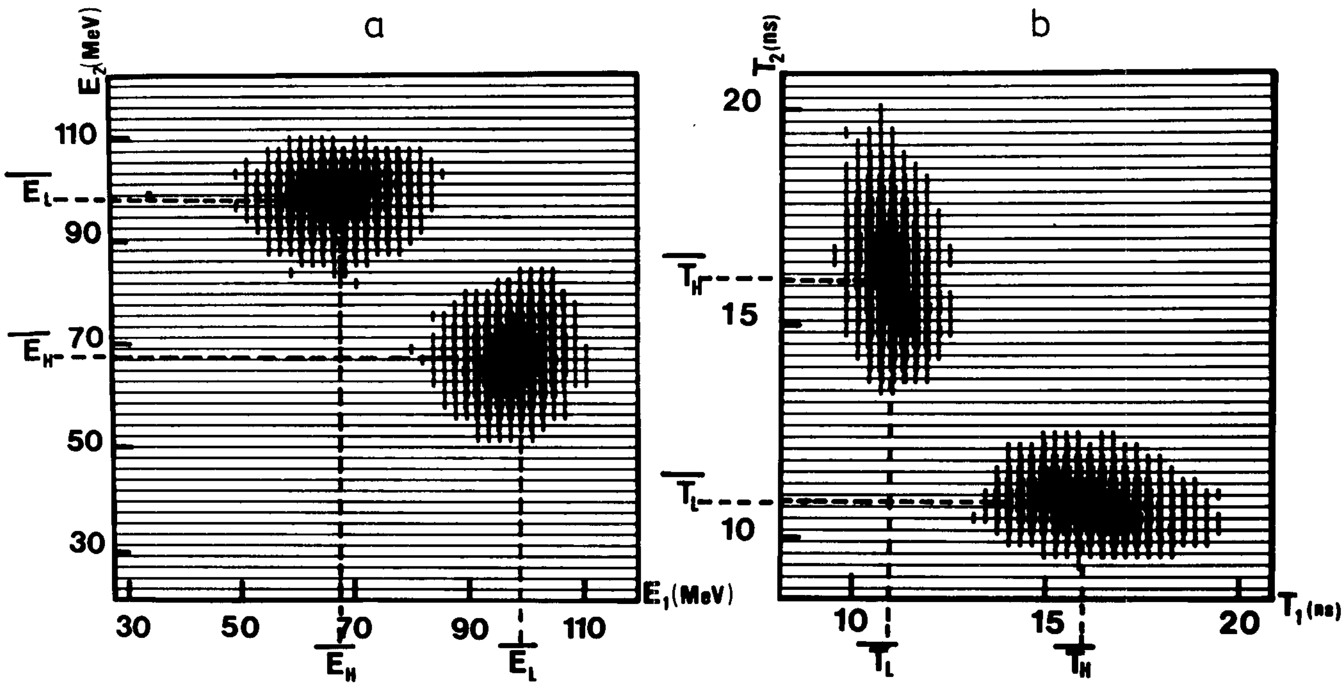

Fig. 5: Bi-parametric contour plots of a) energies and b) velocities of fission fragments from the ^{233}U (d,pf) reaction

References

(1) F. Voß, S. Cierjacks, L. Kropp, Proc. 3rd Conf. on Neutron Cross Sections and Technology, March 1971, Knoxville, Tenn., CONF-710301, p. 218

(2) D.L. Broder, V.E. Kolesov, A.I. Lashuk, I.P. Sadokhin, A.G. Dovbenko, Atom. Energ. 16 (1964) 103

(3) R.E. Coles, Report, AWRE O 41/71 (1971)

(4) G. Grenier, B. Duchemin, D. Parisot, Report, CEA-R-4634 (1974)

(5) R.P. Corcuera, Nucl. Sci. Eng. 58 (1975) 278

(6) J.E. Monahan, A.J. Elwyn, Phys. Rev. Lett. 20 (1968) 1119

(7) Y. Patin, S. Cierjacks, J. Lachkar, J. Sigaud, C. Humeau, J. Chardine, Report, CEA-N-1875, April 1976

2. 3 MV Van-de-Graaff-Accelerator

2.1 Structural Materials

2.1.1 Total Cross Section of ^{58}Fe

H. Beer, Ly Di Hong, F. Käppeler

^{58}Fe is the last isotope investigated in the course of an extensive program for the measurement of total and capture cross sections of structural materials. The transmission of ^{58}Fe was measured by time-of-flight in the neutron energy range from 7 to 320 keV with a time resolution of 0.6 nsec/m (1). Two oxide samples with an enrichment of 65 % were used. The analysis of the transmission data was performed in terms of the R-matrix multilevel formalism by means of a shape fit program taking into account the impurities of the other Fe-isotopes and the oxygen content. Fig. 1 shows the experimental results in the energy interval 32 - 84 keV together with the fitted transmission data. As the sample material contained a considerable amount of ^{56}Fe, strong resonances like that at 74 keV show up in the spectrum. The upper part of Fig. 1 gives the pure total cross section of ^{58}Fe as it is calculated from the resonance parameters.

2.1.2 γ-Production Cross Sections

H. Beer, R.R. Spencer, F. Käppeler

An investigation of high energy γ-rays in keV neutron capture in natural Fe and Ni showed that it was possible to observe those γ-rays for individual resonances and to separate the contributions from different isotopes (2,3). For the determination of absolute partial radiation withs $\Gamma_{\gamma p}$ a careful calibration of the Ge(Li)-efficiency was possible to observe those γ rays for individual resonances and to separate the contributions from different isotopes (2,3). For the determination of absolute partial radiation widths $\Gamma_{\gamma p}$ a careful calibration of the Ge(Li) efficiency was performed with an accuracy of 5-6 % up to γ-energies of 11 MeV (4), using calibrated sources and thermal capture γ-ray lines of known intensities. The resulting $\Gamma_{\gamma p}$ values of 15 transitions for 9 resonances in $^{58,60}Ni$ and ^{56}Fe are listed in Table 1. The related uncertainties range from 12 to 25 %, mainly dependent on the multiple scattering correction.

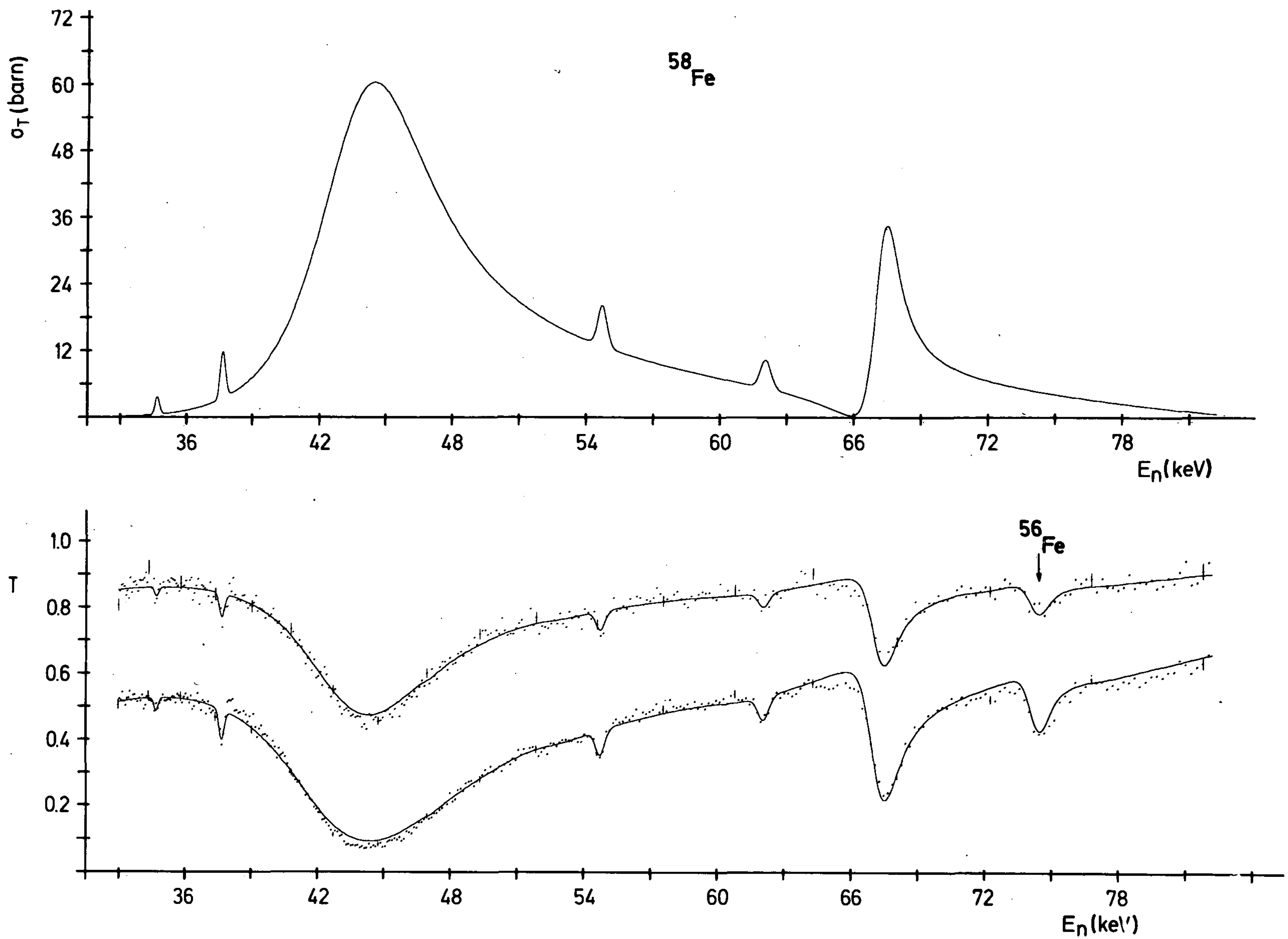

Fig. 1 below: Transmission of ^{58}Fe for two sample thicknesses in the energy range 32-84 keV. The experimental uncertainties are indicated for some points. The solid line represents the the fitted transmission.

above: Total cross section of ^{58}Fe, computed from the resonance parameters.

Target-Nuclide	Resonance Energy (keV)	Spin	E_γ (MeV)	$g \frac{\Gamma_{\gamma p} \Gamma_n}{\Gamma}$ (eV)
^{56}Fe	27.7	1/2	7.67	0.144
			7.66	0.035
	34.1	$1/2^-$	7.68	0.302
	38.3	$1/2^-$ oder $3/2^-$	7.67	0.146
	59.0	$1/2^-$	7.71	0.125
^{58}Ni	15.4	$1/2^+$	9.0	0.124
			8.55	0.110
	32.4		9.03	0.456
			8.15	0.117
	47.8	$3/2^{(-)}$	9.05	0.088
			8.61	0.178
			8.17	0.088
^{60}Ni	12.5	$1/2^+$	7.83	0.514
			7.55	0.289
	47.6	$1/2^-$	7.87	0.285

Table 1: Energies and partial radiation widths of high energy γ-transitions following resonance neutron capture in ^{56}Fe and $^{58,60}Ni$ between 10 and 70 keV

2.2 Main Fissile and Fertile Isotopes

2.2.1 Capture Cross Section of ^{238}U

R.R. Spencer, F. Käppeler

(Relevant to request numbers: 691419, 691435, 692405, 692406, 702032, 714022)

The analysis of the ^{238}U capture cross section measurement relative to the capture cross section of ^{197}Au and the fission cross section of ^{235}U has been completed (5). If the capture cross section of ^{238}U is computed from the ratios using recent evaluations of σ_c ^{197}Au and σ_f ^{235}U, differences between the two data sets of about 5 % were found.

For this reason additional consistency checks of our data analysis will be made to exclude stystematic errors. This would mean then, that the observed 5 % difference is caused by the evaluated cross sections due to the respective uncertainties. Compared to other work, fair agreement is found with the results of de Saussure et al. (6).

2.2.2 Capture to Fission Ratio of ^{235}U

H. Beer, F. Käppeler
(Relevant to request numbers: 691249, 692373, 714008)

With a new technique capture to fission was measured in the neutron energy range between 10 and 500 keV. A large liquid scintillator tank was used to detect capture and fission, while a gas scintillation chamber was placed in front of the tank for measuring the pure fission component. A fission neutron detector inside the tank serves for discrimination between capture and fission events. The data analysis is in progress and it is hoped that the resulting uncertainty will be about 10 %.

2.3 Actinide Cross Sections

2.3.1 Total Cross Sections of $^{240,242}Pu$

F. Käppeler, Ly Di Hong
(Relevant to request numbers: 692439, 712085)

Due to the lack of experimental information on the total cross section of ^{240}Pu and ^{242}Pu in the higher keV-range, a transmission experiment was performed between 20 and 500 keV, using enriched oxide samples. The overall time resolution was 0.8 ns/m and the statistical uncertainty lie between 2 and 4 %. The analysis is not yet completed.

2.3.2 Capture Cross Sections of ^{240}Pu and ^{242}Pu

F. Käppeler, K. Wisshak, G. Rupp
(Relevant to request numbers: 691389, 692451, 692452, 692453, 742010, 712088, 714032, 721137, 671199, 712102, 721098, 721142)

The difficulty in measuring capture cross sections of actinides is the γ-background resulting from natural decay and - in many cases - from fission processes. The technique developed at Karlsruhe works in the energy range of kinematically collimated neutrons. The distance between neutron target and samples is chosen to be only 135 mm in order get a good signal-to-background ratio. Capture events are detected by a Moxon-Rae detector with a time resolution of 1.5 nsec. The radioactive γ-component from the sample is shielded by 0.75 mm lead. ^{235}U and ^{197}Au are used as reference samples, cycled into the beam by a beam-current controlled sample changer. The sample changer also carries a ^{235}U sample for the correction of induced fission events as well as a graphite scatterer and an empty sample container for background corrections. All experimental preperations are finished and the final measurements will start early in 1976.

2.3.3 Fission Cross Section of ^{241}Am

W. Hage[+], H. Hettinger[+], S. Kumpf[+], F. Käppeler
(Relevant to request numbers: 712103, 732115, 742018, 742107)

A measurement of the ^{241}Am fission cross section from threshold to 2 MeV is planned in collaboration with a group from Euratom Ispra. Up to now the gas scintillation chambers for fission fragment detection have been improved towards a better discrimination against α-background. This was achieved by the use of a helium-nitrogen mixture as scintillator gas. A severe difficulty arose from the sample preparation because the thin plastic backings for 4π-detection were destroyed by radiation damage within 3-4 weeks. It is hoped that the life time of new Al-backings will be sufficiently long. In this case, the measurement will start early in summer 1976.

+) Euratom Ispra

References

(1) H. Beer, Ly Di Hong, F. Käppeler, Neutron Interlab Seminar, Geel, Belgium, Nov. 1975
(2) H. Beer, R.R. Spencer, F. Käppeler, 2nd International Symposium on Neutron Capture γ-Ray Spectroscopy, Petten, The Netherlands, Sept. 74
(3) H. Beer, R.R. Spencer, F. Käppeler, Conference on Nuclear Cross Sections and Technology, Washington, March 1975
(4) H. Beer, Neutron Interlab Seminar, Geel, Belgium, Nov. 1975
(5) R.R. Spencer, F. Käppeler, Conference on Nuclear Cross Sections and Technology, Washington, March 1975
(6) G. de Saussure et al., Nucl. Sci. Eng. 51 (1973)

INSTITUT FÜR NEUTRONENPHYSIK UND REAKTORTECHNIK
KERNFORSCHUNGSZENTRUM KARLSRUHE

1. Nuclear Data Evaluation

B. Goel, H. Küsters, E. Stein, F. Weller, F.H. Fröhner
(Relevant to request numbers: 691419, 691435, 692403, 692404, 692405, 692406, 693066, 702032, 714022, 742087, 671203, 691416, 693064, 693065, 712067, 712068, 714020, 732112, 742085, 742136, 692387, 692393, 742083, 691262, 692359, 702025, 691286, 692385, 702029, 714016, 732113, 691319, 692415, 691391, 714028)

KEDAK-3, a new version of the Karlsruhe nuclear data library, was released in September 1975. The main changes with respect to the 1971 version KEDAK-2 are

1. thoroughly revised ^{238}U cross sections above the region of resolved resonances (1), in particular
   - lower σ_γ values (up to 20 % reduction between 4 keV and 15 MeV),
   - lower σ_f values (3 - 6 % reduction above 2 MeV),
   - lower σ_{in} values (about 60 % reduction between 1.4 and 1.8 MeV);
2. thoroughly revised ^{239}Pu cross sections above the resolved resonance region (1), in particular
   - lower σ_T values (2 - 5 % reduction above 200 keV);
3. incorporation and improvements of evaluations by Caner and Yiftah for ^{238}Pu (2), ^{240}Pu (3) and ^{241}Pu (4); ^{242}Pu;
4. revised individual and average resonance parameters for ^{235}U, ^{238}U, ^{239}Pu and ^{240}Pu. The average resonance parameters (cf. Table I) are now consistent (within reasonable confidence limits) with individual resonance parameters for l = 0 and with average cross section data up to about 200 keV for l = 1 and l = 2.

For more details see Table 2 and Ref. (5).

Details of the ^{238}U and ^{239}Pu evaluation were reported at the 1975 Washington Conference (1) together with integral checks of the new ^{235}U, ^{238}U, ^{239}Pu, ^{240}Pu, ^{241}Pu and ^{242}Pu data by means of k_{eff} calculations for a variety of different critical assemblies. These checks showed that, while KEDAK-2 leads to about 1-5 % underprediction, KEDAK-3 yields roughly 0-1 % underprediction. The construction of group constant sets directly from microscopic data, without further need for adjustment by means of integral data, appears thus to become a possibility in the foreseeable future, at least as far as the prediction of k_{eff} is concerned.

References

(1) B. Goel, H. Küsters and F. Weller, Proc. Int. Conf. on Nuclear Cross Sections and Technology, Washington 1975

(2) M. Caner and S. Yiftah, Report IA-1301 (1974)

(3) M. Caner and S. Yiftah, Report IA-1243 (1972)

(4) M. Caner and S. Yiftah, Reports IA-1275 (1973) and IA-1276 (1973)

(5) B. Goel and B. Krieg, Report KFK 2234 (1975)

Table 1: KEDAK-3, revised average resonance parameters

Isotope	ℓ	J	$\bar{\Gamma}_\gamma$ (meV)	$\bar{\Gamma}_n^\ell$ (meV)	$\bar{\Gamma}_n^\ell/D$ (10^{-4})	D (eV)	R' (fm)
^{235}U	0	3	48	.102	.93	1.09	9.65
	0	4	48	.102	.93	1.09	
	1	2	48	.192	2.0	.96	
	1	3	48	.252	2.0	1.26	
	1	4	48	.252	2.0	1.26	
	1	5	48	.282	2.0	1.41	
^{238}U	0	1/2	24	1.879	.93	20.20	9.30
	1	1/2	24	3.640	1.8	20.20	
	1	3/2	24	1.879	1.8	10.17	
	2	3/2	24	.946	.93	10.17	
	2	5/2	24	.635	.93	6.83	
^{239}Pu	0	0	43	1.110	1.25	8.86	9.05
	0	1	43	.393	1.25	3.14	
	1	0	43	2.040	2.3	8.86	
	1	1	43	.722	2.3	3.14	
	1	2	43	.492	2.3	2.14	
^{240}Pu	0	1/2	30.6	1.175	.94	12.5	9.30
	1	1/2	30.6	2.380	1.9	12.5	
	1	3/2	30.6	1.196	1.9	6.293	
	2	3/2	30.6	.592	.94	6.293	
	2	5/2	30.6	.397	.94	4.225	

Table 2: Status of the evaluation for different KEDAK-3 materials

Material name	References	Comments
H 1		Only ISOT 1 and ISOT 2 are available
H H1 (H bound in H_2) H 01 (H bound in H_2O)	J.J. Schmidt KFK 120 (1966) R. Meyer KFK 1272/2 (1972) p. 122-12 ff B. Goel 1975 to be published	1971: Data extended to 15 MeV Revision of data for σ_t above 700 keV, σ_c throughout the energy range (0.001 eV to 15 MeV), angular distribution for elastic scattering and μ_1. 1975: σ_t and $\sigma(n,n)$ revised below 700 keV, for H 01
H 2 (D)	J.J. Schmidt KFK 120 (1966) B. Goel 1975 to be published	1975: Data extended to 15 MeV and revised for σ_c, σ_t, σ_n and $\sigma(n,2n)$ above 1 keV
HE 3	J.J. Schmidt KFK 120 (1966)	Only data for $\sigma(n,p)$ available between 0.01 keV and 10 MeV.
HE 4	J.J. Schmidt KFK 120 (1966)	Data only upto 10 MeV
C 12	J.J. Schmidt KFK 120 (1966) R. Meyer KFK 1272 (1972) B. Goel 1975 to be published	1971: Data extended to 15 MeV. Revision of data for $\sigma(n,n')$, $\sigma(n,p)$, $\sigma(n,\alpha)$, $\sigma(n,3\alpha)$ and 4 levels of inelastic scattering 1975: Data revised for σ_c above 1 eV and σ_t below 1.4 MeV

Material name	References	Comments
N	B. Hinkelmann et al. KFK 1340 (1971)	Only angular distributions of neutron elastic scattering for 48 energies between 100 keV and 15.8 MeV are available
^{16}O	J.J. Schmidt KFK 120 (1966) F. Weller and B. Goel 1975 to be published	1975: Data extended to 15 MeV. Data revised for scattering cross sections, σ_c, $\sigma(n,p)$, $\sigma(n,d)$ and $\sigma(n,\alpha)$
^{23}Na	J.J. Schmidt KFK 120 (1966) R. Meyer, Internal Report (1973) B. Goel 1975 to be published	1970: Data extended to 15 MeV. New evaluation for $\sigma(n,p)$, $\sigma(n,\alpha)$, $\sigma(n,2n)$ and σ_c above 1 MeV. 1971: Reevaluation of Resonance data in the energy range 1 keV to 60 keV 1975: Scattering data revised above 4 MeV and σ_c revised between 60 keV and 1 MeV
^{27}Al	J.J. Schmidt KFK 120 (1966) B. Hinkelmann et al. B. Goel 1975 to be published	1967-1969: Reevaluation of data for resolved and statistical resonance parameter, elastic scattering and its angular distribution above 100 keV. 1975: Data for 5.9 keV resonance revised, σ_c revised between 0.1 eV and 7 keV. The data for $\sigma(n,n')$, $\sigma(n,p)$ and $\sigma(n,\alpha)$ are also modified above 10 MeV.

Material name	References	Comments
CL	B. Schatz unpublished	Data originates from UNC-5067 (1963)
CL 35 CL 37		Only ISOT1 and ISOT2 are available
CR	J.J. Schmidt KFK 120 (1966) R. Meyer, Internal Report (1970) B. Goel 1975 to be published	1970: Data extended to 15 MeV Data improved for σ_c above 1 MeV and for $\sigma(n,p)$, $\sigma(n,\alpha)$ and $\sigma(n,2n)$ 1975: Data revised for σ_c above 100 keV and $\sigma(n,n')$ above 4 MeV
CR 50 CR 52 CR 53 CR 54	R. Meyer, Internal report (1970)	Only data for resonance parameters, $\sigma(n,p)$, $\sigma(n,\alpha)$, $\sigma(n,2n)$, ISOT1 and ISOT2 are available
FE	J.J. Schmidt KFK 120 (1966) R. Meyer, Internal report (1970)	1970: Data extended to 15 MeV Reevaluation of σ_c above 1 MeV and of $\sigma(n,p)$, $\sigma(n,\alpha)$ and $\sigma(n,2n)$ 1975: Data are being revised
FE 54 FE 56 FE 57 FE 58	R. Meyer, Internal report (1970)	Only data for resonance parameter, $\sigma(n,\alpha)$, $\sigma(n,2n)$, ISOT1 and ISOT2 are available. Only data for $\sigma(n,p)$, $\sigma(n,\alpha)$, average level spacing, ISOT1 and ISOT2 are available
Ni	J.J. Schmidt KFK 120 (1966) R. Meyer, Internal report (1970) B. Goel 1975 to be published	1970: Data extended to 15 MeV. Reevaluation of σ_c above 1 MeV and of $\sigma(n,p)$, $\sigma(n,\alpha)$ and $\sigma(n,2n)$ 1975: σ_c revised above 200 keV. $\sigma(n,n')$ revised above 4 MeV

Material name	References	Comments
Ni 58 Ni 60 Ni 61 Ni 62 Ni 64	R. Meyer, Internal report (1970)	Only data for resonance parameters, $\sigma(n,p)$, $\sigma(n,\alpha)$, $\sigma(n,2n)$, ISOT1 and ISOT2 are available
MO	J.J. Schmidt KFK 120 (1966) R. Meyer Internal report (1973)	1970: Data extended to 15 MeV. Reevaluation of σ_c above 1 MeV, and of $\sigma(n,p)$, $\sigma(n,\alpha)$ and $\sigma(n,2n)$
MO 92 MO 94 MO 95 MO 96 MO 97 MO 98 MO 100	R. Meyer Internal report (1973)	Data available only for resonance parameters, $\sigma(n,p)$, $\sigma(n,\alpha)$, $\sigma(n,2n)$, ISOT1 and ISOT2
CD	J.J. Schmidt KFK 120 (1966)	No change in data except that mentioned in introduction
U 235	J.J. Schmidt KFK 120 (1966) B. Schatz KFK 1629 (1973) F. Weller and B. Goel 1975 to published	1973: New evaluation of $\bar{\nu}$ and all other data above the resolved resonance region. 1975: New evaluation of σ_f and σ_t above 100 keV
U 238	J.J. Schmidt KFK 120 (1966) B. Goel, H. Küsters and F. Weller Wash.-Conference 1975 and specialist meeting Harwell 1975 and to be published	1975: Extensive revision of all the data
Pu 238	M. Caner and S. Yiftah IA 1301 (1974) B. Goel and B. Krieg 1975 to be published	New material on KEDAK

Material name	References	Comments
Pu 239	J.J. Schmidt KFK 120 (1966) B. Hinkelmann et al. KFK 1340 (1971) B. Goel, H. Küsters and F. Weller, Washington Conf. 1975 and to be published	Extensive revision of most of data
Pu 240	M. Caner and S. Yiftah IA-1243 (1972) F. Weller, B. Goel and F. Fröhner 1975 to be published	1975: New evaluation of resonance parameters and storage of pointwise data in resonance region
Pu 241	M. Caner and S. Yiftah IA 1275 (1973) and IA 1276 (1973)	1975: Storage of pointwise cross sections in the resonance region
Pu 242	F. Weller 1975 to be published	

2. Shape Analysis of Structural-Material Capture Data

F.H. Fröhner

(Relevant to request numbers: 692102, 714605, 721041, 721042, 702009, 691128)

Previously reported neutron capture data on ^{56}Fe, ^{58}Ni, ^{60}Ni and ^{61}Ni (1) measured at the Karlsruhe 3 MV Van de Graaff accelerator were analyzed with a newly developped capture shape analysis program. Figs. 1-3 show the R-maxtrix multi-level fits including Monte-Carlo-calculated multiple-interaction yields and resolution broadening. A rather complete parametrization including Γ_γ (or, for narrow levels, $g\Gamma_n\Gamma_\gamma/\Gamma$) values was achieved up to 160 keV for the even target nuclides and up to 30 keV for ^{61}Ni. Tables 1-3 show the results obtained for s-wave resonance capture which were reported (2) at the 1975 Washington Conference. The following conclusion could be drawn:

- The shape of the broad 12.3 keV capture peak of ^{60}Ni+n could be fitted very well without a channel capture contribution. Claims that the shape of this resonance cannot be explained without a channel capture component (3) are not substantiated by the present results.
- The same is true for suggestions that the apparent residual capture cross section between resonances is due to potential capture. The calculations show that it is due to resonance capture of scattered neutrons, mostly in the sample itself but also in the bronce container and the aluminium beam tube of the scintillator tank.
- A significant Γ_n^o-Γ_γ-correlation was found only for ^{60}Ni where it is almost wholly due to the 12.3 keV resonance.

References

(1) A. Ernst, F.H. Fröhner and D. Kompe, Nuclear Data for Reactors, IAEA, Vienna 1970, vol. I, p. 633

(2) F.H. Fröhner, Nuclear Cross Sections and Technology, NBS Spec. Publ. 425 (1975), vol. II, p. 929

(3) M. Lubert, N.C. Francis and R.C. Block, Nucl. Phys. A230 (1974) 83

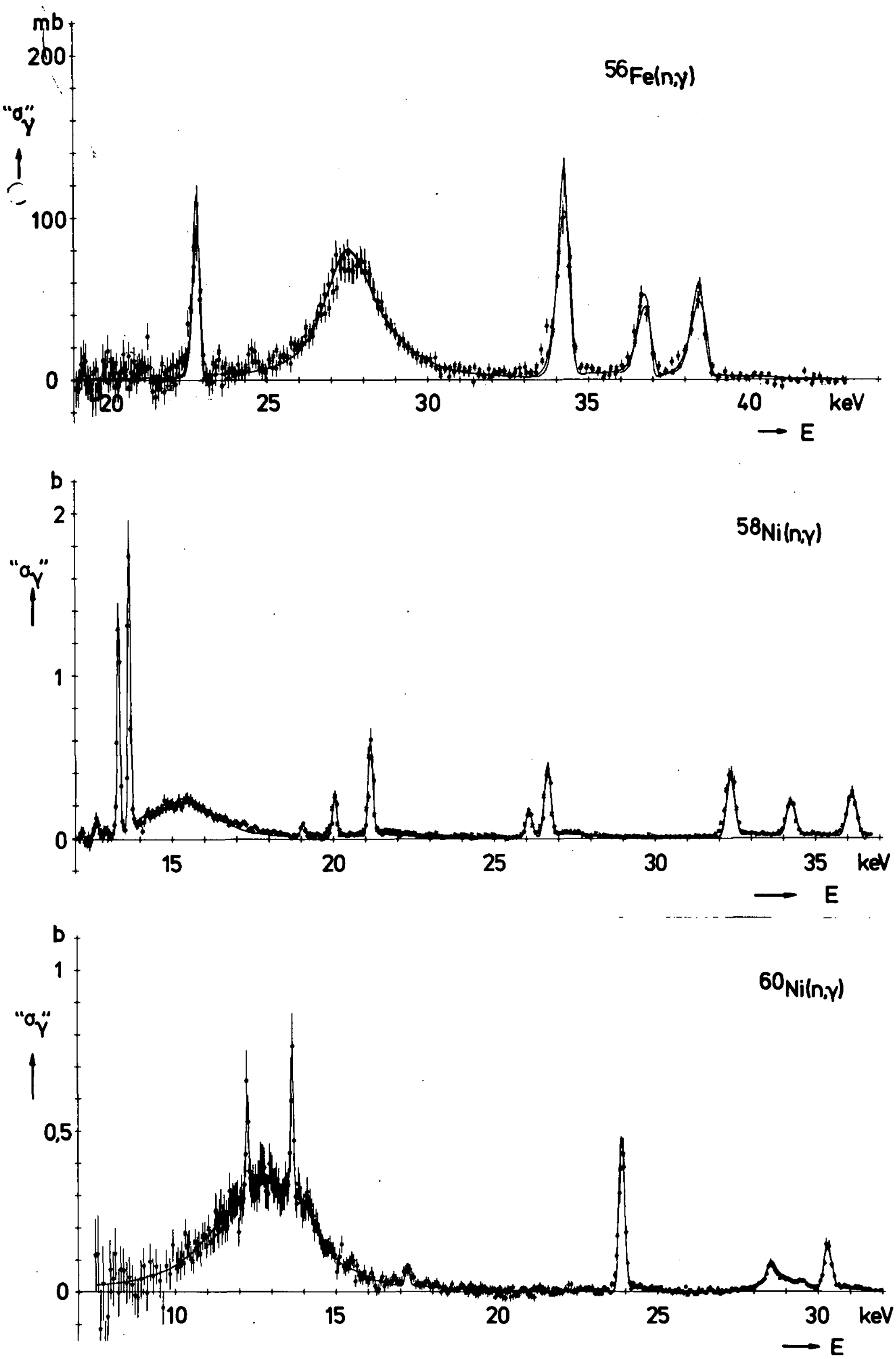

Fig. 1: Experimental capture data (point symbols with error bars) and multi-level R matrix fits (solid lines). Enriched samples: 99.7 % ^{56}Fe, .00992 nuclei/b; 99.9 % ^{58}Ni, .01057 nuclei/b; 99.8 % ^{60}Ni, .01022 nuclei/b

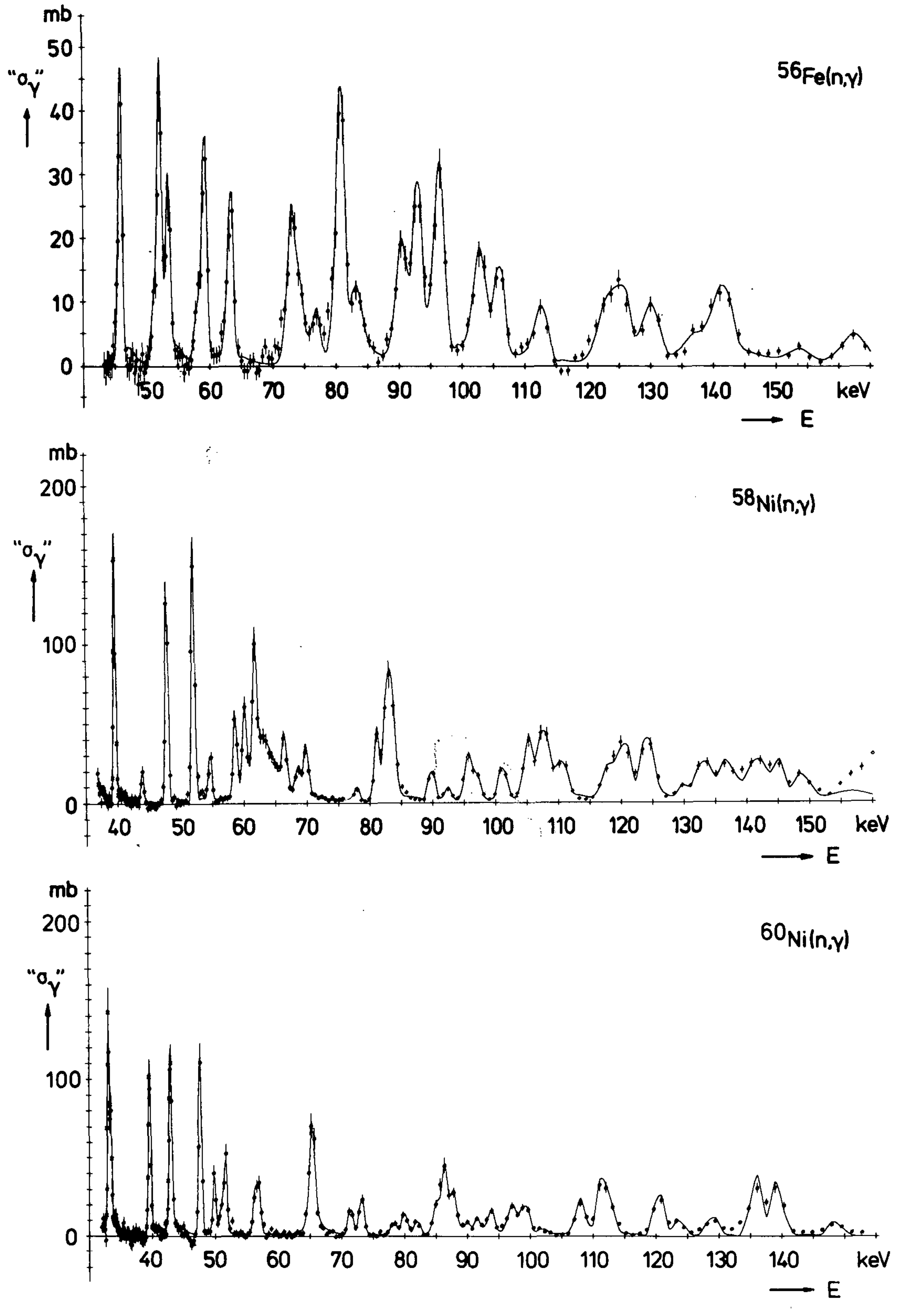

Fig. 2: Experimental capture data (point symbols with error bars) and multi-level R matrix fits (solid lines). Enriched samples:
99.7 % ^{56}Fe, .00992 nuclei/b; 99.9 % ^{58}Ni, .01057 nuclei/b;
99.8 % ^{60}Ni, .01022 nuclei/b

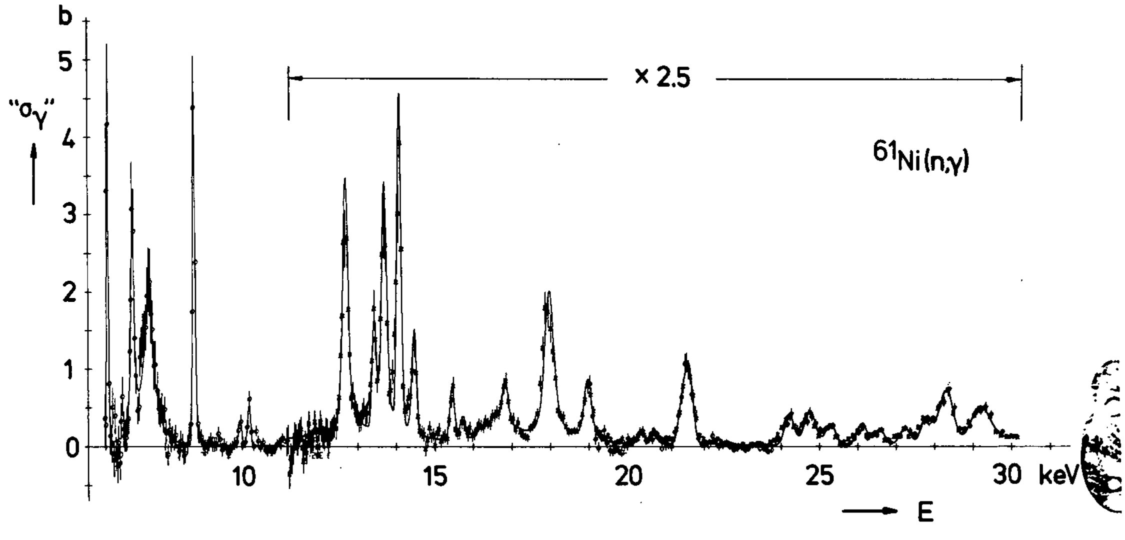

Fig. 3: Experimental capture data (point symbols with error bars) and multi-level R matrix fits (solid lines). Enriched sample: 91.8 % ^{61}Ni, 0.00460 nuclei/b

Table 1: Parameters of s-wave resonances for even isotopes

Target nucleus	E_0 (keV)	Γ_n (eV)	Γ_γ (eV) area RPI[6,7]	area KFK[1,2]	shape KFK
^{56}Fe	27.6 ± .2	1400 ± 70	1.44 ± .14	1.4 ± .2	1.18 ± .15
	73.8 ± .5	540 ± 40			.62 ± .15
	83.2 ± .3	960 ± 80		.9 ± .3	.55 ± .22
	129.8 ± .4	500 ± 50			1.12 ± .16
	140.7 ± .5	2370 ± 200			1.20 ± .35
^{58}Ni	15.4 ± .1	1200 ± 30		2.1 ± .7	1.42 ± .18
	63.0 ± .2	3600 ± 200		3.2 ± .8	2.3 ± .3
	107.6 ± .3	1400 ± 300		3.3 ± .8	3.8 ± .9
	124.0 ± .5	700 ± 250		3.0 ± .6	3.5 ± .6
^{60}Ni	12.3 ± .1	2660 ± 100	3.30 ± .30	3.3 ± .4	2.65 ± .28
	28.6 ± .1	800 ± 50	1.1 ± .1	1.2 ± .3	.6 ± .15
	42.9 ± .1	120 ± 30	1.73 ± .30	1.0 ± .2	.92 ± .18
	65.4 ± .2	500 ± 150	2.43 ± .25	1.8 ± .3	1.79 ± .26
	86.3 ± .2	330 ± 25		1.5 ± .3	1.51 ± .30
	97.2 ± .3	1000 ± 200		1.0 ± .3	1.13 ± .20
	108.0 ± .3	700 ± 100		1.1 ± .3	1.35 ± .20
	155.4 ± .5	440 ± 50		.8 ± .3	.85 ± .17
	161.7 ± .5	1400 ± 200		1.8 ± .5	1.9 ± .4

Table 2: Parameters of s-wave resonances, ^{61}Ni

Target nucleus	E_0 (keV)	J	Γ_n (eV)	Γ_γ (eV) area KFK[1]	shape KFK
^{61}Ni	7.15 ± .02	1	74 ± 8	2.5 ± .5	2.55 ± .35
	7.58 ± .02	2	177 ± 16	2.3 ± .6	2.23 ± .35
	8.75 ± .02	2	6 ± 2	2.6 ± .8	2.31 ± .60
	12.67 ± .03	2	75 ± 4	1.7 ± .4	1.72 ± .25
	13.68 ± .05	2	61 ± 4	1.6 ± .4	1.65 ± .25
	14.06 ± .05	1	17 ± 4	3.1 ± .5	3.20 ± .45
	16.61 ± .10	1	817 ± 16	2.2 ± .4	2.07 ± .30
	17.99 ± .10	1	177 ± 8	1.6 ± .5	1.4 ± .4
	18.97 ± .10	2	69 ± 4	.9 ± .3	.78 ± .11
	24.73 ± .07	1	129 ± 10	1.4 ± .3	1.41 ± .20
	28.35 ± .07	2	5 ± 4	3.0 ± 1.0	2.2 ± .8
	29.3 ± .1	1	409 ± 22	2.4 ± .4	1.6 ± .3

Table 3: Width correlation coefficients calculated from shape analysis results

Target nucleus	J	Sample size	$\frac{\mathrm{cov}\{\Gamma_n^o, \Gamma_\gamma\}}{\sqrt{\mathrm{var}\{\Gamma_n^o\} \cdot \mathrm{var}\{\Gamma_\gamma\}}}$
^{56}Fe	1/2	5	+ 0.55 ± 0.65
^{58}Fe	1/2	4	- 0.74 ± 0.77
^{60}Ni	1/2	9	+ 0.71 ± 0.26
^{61}Ni	1	6	- 0.19 ± 0.37
	2	6	+ 0.10 ± 0.51

3. Preequilibrium Model Development

H. Jahn, C.H.M. Broeders and I. Broeders
(Relevant to request number: 742030)

The theory of preequilibrium decay processes of the compound nucleus as developped by Blann for inelastic proton scattering (1) should be applicable also to inelastic scattering of neutrons in the MeV region. Our attempts to interpret the observed spectrum of inelastically scattered neutrons from the $^{56}Fe(n,n')$ reaction induced by 14.7 MeV neutrons were, however, only partially successful (2). It was found that the theory as formulated in ref. (1) could not reproduce the observed energy distribution without parameter adjustment, although it is supposed to yield absolute values. Furthermore, the observed angular distributions suggest that Blann's original addition of an evaporation and a preequilibrium component should be extended to include a third, direct component. Results ontained in a first attempt with the semiclassical theory of direct processes (Butler et al. (3) were encourageing. The angular distributions of inelastically scattered neutrons could be fitted at least in the range where semiclassical theory is applicable, i.e. for relatively large scattering angles, without need to change the parameters of Blann's model.

In order to remove the restriction to large angles we replaced the semiclassical treatment by the plane-wave Born approximation (PWBA) following Austern et al. (4). The double-differential scattering cross section can then be expressed as

$$\frac{d^2\sigma(E,E',\theta)}{d\Omega dE'} = \left(\frac{d\sigma(E,E')}{4\pi dE'}\right)_{evap} + \left(\frac{d\sigma(E,E')}{4\pi dE'}\right)_{Blann} + \left(\frac{d\sigma(E,E',\theta)}{d\Omega}\right)_{direct} \qquad 1$$

with the equilibrium part

$$\left(\frac{d\sigma(E,E')}{4\pi dE'}\right)_{evap} = C\ \sigma_r(E')E'e^{-E'/T},\ T = \sqrt{\frac{E}{\nu A}} \qquad 2$$

(σ_r: optical-model reaction cross section, C: constant fit parameter, ν : evaporation temperature parameter, A: nucleon number) and the direct-reaction part

$$\left(\frac{d\sigma(E,E',\theta)}{d\Omega}\right)_{direct} = \mathrm{const}\sqrt{\frac{E'}{E}}\ (2\ell'+1)\ \sum_L C_{\ell\ell'}(L,0;\ 0,0)\cdot j_L(QR)^2 \qquad 3$$

($\hbar\vec{Q} = h(\vec{k}-\vec{k}')$: momentum transfer; $\hbar\vec{L} = \hbar(\vec{\ell}-\vec{\ell}')$: angular momentum transfer; ℓ,ℓ': angular-momentum quantum numbers of the directly reacting target nucleon before and after the collision; j_L: sherical Bessel function; $C_{\ell\ell'}$: Clebsch-Gordan coefficient). The same expression 3 is valid if collective excitations instead of independent-particle excitations are considered, with ℓ,ℓ', L denoting the corresponding collective-state angular-momentum quantum numbers. A closer inspection of the predominating individual-particle and collective excitations shows that mainly terms with L = 2 contribute. Fig. 1 illustrates the quality of the fits to measured angular distributions which are obtained with the L = 2 terms alone, i.e. with a pure $j_2(QR)^2$ dependence of the direct component. Angle-integrated results are shown in Fig. 2 (5). On the basis of these results it is concluded that in addition to evaporation and preequilibrium processes a third, direct-reaction component is required. A relatively simple (PWBA) formulation of the direct-reaction term is shown to be adequate for a reproduction of observed angular and angle-integrated data.

Recently Blann modified his model by replacing the originally employed equidistant one-nucleon level density by a more realistic Fermi-gas level density (6). The consequences on our results are being investigated.

References

(1) M. Blann, Nucl. Phys. A213 (1973) 570

(2) C.H.M. Broeders, I. Broeders, H. Jahn, M. Lalović, Report NEANDC(E) 162U (1975)

(3) S.T. Butler, N. Austern and C. Pearson, Phys. Rev. 112 (1958) 1227

(4) N. Austern, S.T. Butler and Mc Manus, Phys. Rev. 92 (1953) 350

(5) H. Jahn, C.H.M. Broeders and I. Broeders, Nuclear Cross Sections and Technology, NBS Spec. Publ. 425 (1975), vol. I, p. 350

(6) M. Blann, Report UR-NSRL-92 (1974)

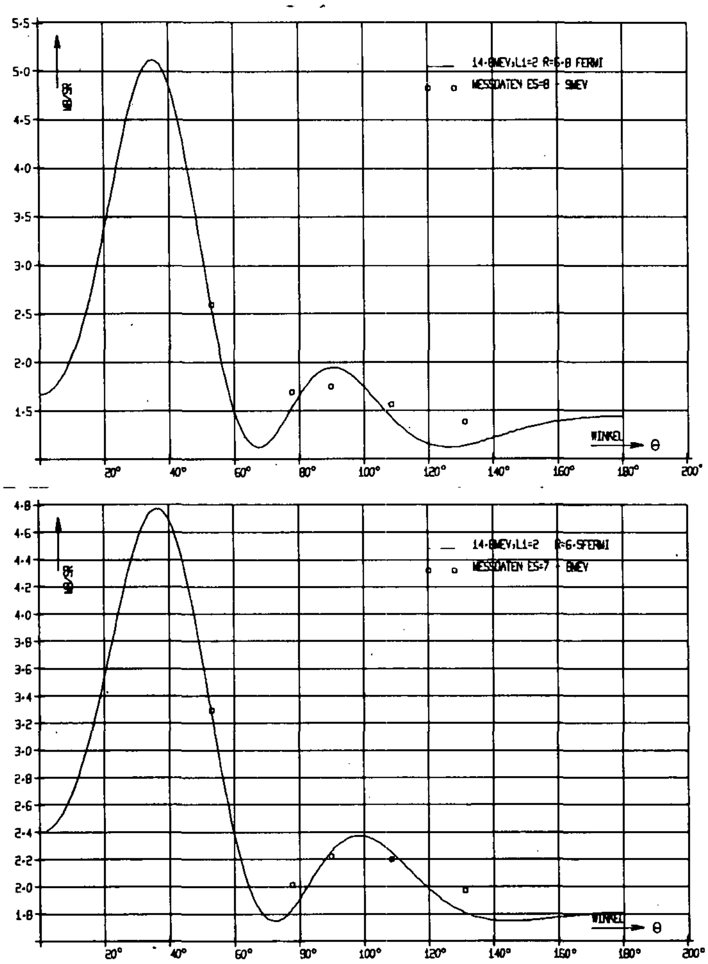

Fig. 1: PWBA-fit of angular distributions of 14.7 keV neutrons scattered inelastically by ^{56}Fe. Upper curve 10-11 MeV, lower curve 7-8 MeV

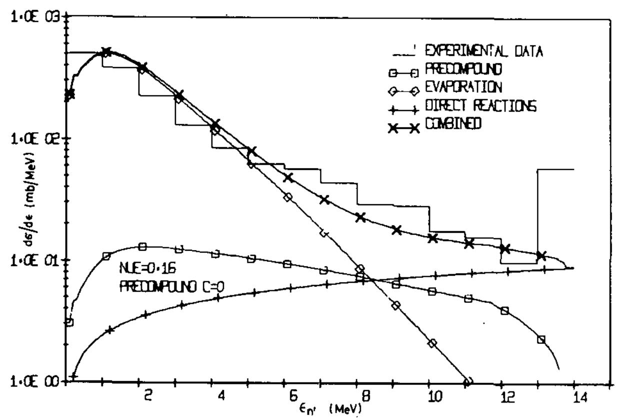

Fig. 2: Comparison between measured and calculated angular integrated inelastic cross sections, where the fit includes the direct part (ν = 0.16 see equ. (2)).

INSTITUT FÜR RADIOCHEMIE
KERNFORSCHUNGSZENTRUM KARLSRUHE

Excitation Functions of ^{3}He-Reactions with Y and Nb

S. Flach and H. Münzel

Despite the fact that the number of mashines for accelerating ^{3}He did increase considerably in the last years there were up to now only rather few excitation functions measured for ^{3}He-reactions. Consequently, the half empirical systematics of excitation functions (1) published in 1974 did contain for many ^{3}He-reactions only rough guesses. Therefore we have in the frame of new research program determined for projectile energies up to 40 MeV the excitation functions for the following reactions (3).

^{93}Nb(^{3}He,xn)$^{96-x}$Tc (x=2,3,4) ^{93}Nb(^{3}He,α2n)^{90}Nb

^{93}Nb(^{3}He,p2n)^{93}Mo

^{89}Y(^{3}He,xn)$^{92-x}$Nb (x=2,3,4) ^{89}Y(^{3}He,2p)^{90}Y

^{89}Y(^{3}He,pxn)$^{91-x}$Zr (x=2,3) ^{89}Y(^{3}He,αxn)^{88}Y (x=0,1,2)

In Fig. 1 some of the results are shown. The measured values are compared with calculated cross sections using a combination of the compound- and the precompound-reaction model. The agreement between experimental and calculated values is not very satisfactory (see Fig. 2). In general the emission of protons is overestimated, which is probably due to the magic number N=50.

Karlsruher Nuklidkarte

The 4th edition of the Karlsruher Chart of Nuclides covering the literature up to April 1974 was prepared. Compared to the 3rd edition only minor changes were introduced. Again two sizes are available: the wall chart and a folded chart. Due to high demand the 15 000 copies printed of each kind are already distributed but an unchanged reprint will be available soon.

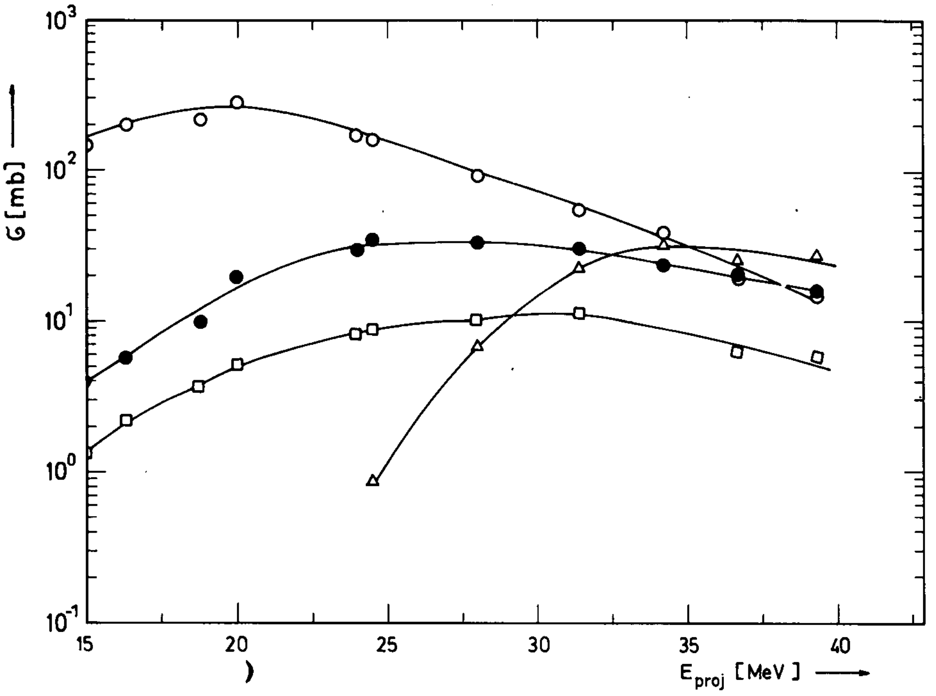

Fig. 1: Excitation functions for the following reactions:
O: $^{89}Y(^3He,2n)^{90m+g}Nb$ □: $^{89}Y(^3He,2p)^{90m}Y$
●: $^{89}Y(^3He,\alpha n)^{87m}Y$ Δ: $^{89}Y(^3He,\alpha 2n)^{86m}Y$

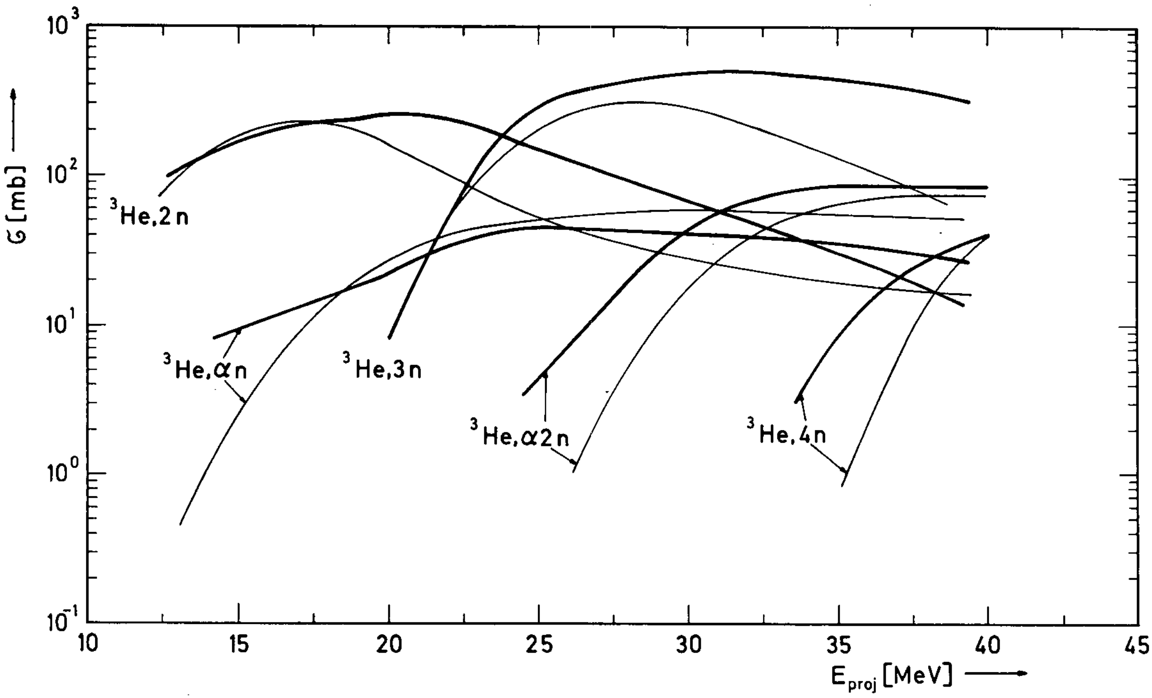

Fig. 2: Comparison of experimentally determined excitation functions (▬▬) for ^{3}He-reactions on ^{89}Y with calculated curves (———)

KACHAPAG-File

Since several years the Karlsruher Charged Particle Group (KACHAPAG) is compiling cross sections and thick target yields for charged particle induced reactions. A summary was prepared in 1973 (2). Now the data are stored on magnetic tape for easier handling. For this purpose an improved version of the EXFOR-Format, which was originally developed for the compilation of neutron data, is used.

References

(1) H. Münzel, J. Lange, K.A. Keller, Landolt-Börnstein: Zahlenwerte und Funktionen aus Naturwissenschaften und Technik, N.S. Gruppe 1, Bd. 5c; Springer Verlag, Berlin, Heidelberg, New York, 1974

(2) J. Lange, H. Münzel, K.A. Keller, G. Pfennig, ibid., Bd. 5b; Springer Verlag, Berlin, Heidelberg, New York, 1973

(3) S. Flach, Thesis, University Karlsruhe, 1976

EUROPEAN INSTITUTE FOR TRANSURANIUM ELEMENTS
KARLSRUHE, F.R. GERMANY

Measurement of Integral Neutron Reaction Rates and Cumulative Fission Yields for U-235 in a Fast Reactor Neutron Flux

G. Cottone, A. Cricchio, L. Koch

In the frame of the R and D programme of the EUROPEAN INSTITUTE for TRANSURANIUM ELEMENTS, KARLSRUHE, an experiment, TACO, was performed in order to determine the neutron reaction rates for heavy nuclides (^{232}Th to ^{243}Am) in the fast reactor, RAPSODIE. In addition, the cumulative fission yields of these fission sources were determined. The results pertinent to ^{235}U have been finally evaluated. They are derived from two separately irradiated capsules each containing about 10 mg of this isotope.

1. Neutron Reaction Rates

The neutron reaction rates were evaluated according to the described formulas (Table I). In order to avoid errors caused by the loss of material during handling, we desisted from comparing the initial amount of the fuel with the final number of atoms after irradiation. Instead, we determined the initial amount from the post-irradiation analyses by summing up all heavy nuclides and the fission products. We had to measure the fission yields of ^{148}Nd for this purpose. The results obtained for the neutron capture and fission reaction rates as well as the (n,2n) reaction rates, are summarized in Table I.

2. Cumulative Fission Product Yields for ^{235}U

The cumulative fission product yields for the heavy mass range above the mass number of 117, were determined by normalizing the fission product abundance to 200 %. Through the use of isotope dilution mass-spectrometry and gamma spectrometry, selected fission products were determined. Yields for the masses in the range of 116.8 to 124, 126 to 130, 138 to 142, and 147 were interpolated with the aid of recommended thermal fission yields. An interpolation with the recently published EBR II data (1) would significantly reduce all the fission yields of the nuclides by 0.7 %. Because of our experience gained in the determination of ^{138}Ba and ^{140,142}Ce through isotope dilution mass-spectrometry, we prefer the thermal fission yields. Any results obtained by this technique are doubtful though, due to the extreme difficulties caused by contamination of natural elements. However, this technique was applied for the EBR II analysis.

Except for the lowest yields and the masses 135 and 143 there is an agreement between the fission yields obtained and the new EBR II fission yields (Table II). The difference is obviously due to the change in the neutron energy spectrum which, in the case of ^{143}Nd, can be clearly seen in the figure. With an increase in the energy of the fission inducing neutron, the fission yield of only this Nd isotope drops significantly. This may be so because it is on one of the peaks of the fine structure. The agreement with previously published fission yields is poor (2,3,4).

The main objective of the TACO experiment is to determine fission yields for precise burn-up measurements in fast reactors. In this respect, it can be concluded that the ^{148}Nd fission yields for the RAPSODIE and DFR reactor are 1.665 % (Table II). As the deviation for the thermal fission yield (1.68 %) is small, it can be assumed that the larger fast reactors of the PHENIX or PFR type, will have a ^{148}Nd fission yield of 1.67 $\pm$ 0.01 %.

References

(1) W.J. Maeck, ICP-1050-1 (1975)

(2) W. Davies, Radiochimica Acta **12** (1969) 173

(3) W.J. Maeck, et al., ICP-1058 (1974)

(4) J.M. Chaumont, et al., ANS Meeting, Jackson Lake Lodge, Wy., (1973)

Table I: Neutron Reaction Rates and α-values for ^{235}U

	TACO 33	TACO 34
$\sigma_a \emptyset\ t = -\ln \left[\frac{N\,\Sigma\,(No)i}{No\ (\Sigma Ni + \frac{N_{Nd}}{Y})} \right]$	0.0897	0.0897
$\sigma_f \emptyset\ t = \frac{\sigma_a \emptyset\ t \sum (No)_i / (1 + Y \frac{\Sigma Ni}{N_{Nd}})}{No\ [1-\exp(-\sigma_a \emptyset\ t)]}$	0.0744	0.0743
$A\ \sigma_c^I\ \emptyset\ t = \frac{\frac{^{A+1}N}{N} \exp(-^{A}\sigma_a\ \emptyset\ t) - \frac{^{A+1}No}{No} \exp(-^{A+1}\sigma_a\ \emptyset\ t)}{\exp(-^{A}\sigma_a\ \emptyset\ t) - \exp(-^{A+1}\sigma_a\ \emptyset\ t)} (^{A+1}\sigma_a - {}^{A}\sigma_a)\ \emptyset\ t$	0.0154	0.0151
$\sigma_c^{II} \emptyset\ t = \sigma_a \emptyset\ t - \sigma_f \emptyset\ t$	0.0153	0.0154
$\sigma_{n,2n}\ \emptyset\ t$	$1.07 \cdot 10^{-4}$	$2.8 \cdot 10^{-4}$
$\alpha^I = \sigma_c^I \emptyset\ t / \sigma_f \emptyset\ t$	0.207	0.203
$\alpha^{II} = \sigma_c^{II} \emptyset\ t / \sigma_f \emptyset\ t$	0.206	0.207

Mass Nr.	TACO 33	TACO 34	ERB-II	Mass Nr.	TACO 33	TACO 34	ERB-II
116.8 -124	(0.250	0.252)	0.14	140	(5.05	6.07)	6.19
125	0.053	0.064	0.038	141	(5.55	5.59)	5.85
126	(0.098	0.099)	0.071	142	(5.61	5.64)	5.78
127	(0.199	0.200)	0.151	143	5.69	5.65	5.80
128	(0.494	0.496)	0.372	144	5.23	5.12	5.27
129	(1.09	1.09)	0.840	145	3.75	3.72	3.83
130	(2.00	1.99)	1.71	146	2.93	2.90	2.94
131	3.23	3.19	3.18	147	2.16	2.07	2.11
132	4.66	4.70	4.60	148	1.66	1.67	1.68
133	6.81	6.90	6.82	149	1.01	1.02	1.02
134	7.56	7.60	7.67	150	0.683	0.677	0.672
135	6.73	6.71	6.52	151	0.424	0.403	0.406
136	6.22	6.17	6.16	152	0.230	0.258	0.265
137	6.29	6.25	6.21	153	0.178	0.151	0.168
138	(6.68	6.71)	6.66	154	(0.067	0.067)	0.072
139	(6.36	6.52)	6.76	155	(0.054	0.053)	0.07

Table II: Cumulative fission yields for ^{235}U in the mass range 125-155 (values in brackets are interpolated)

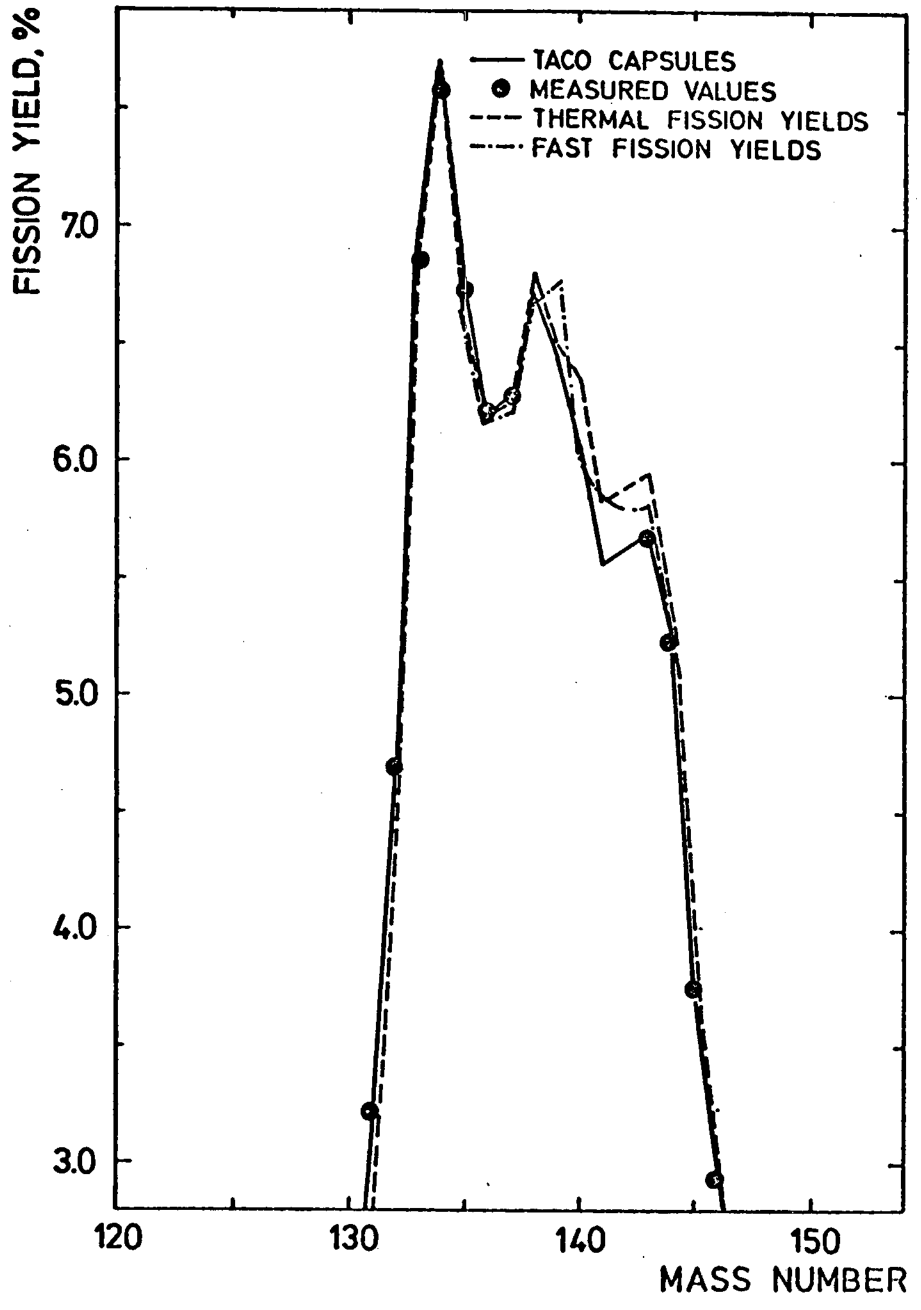

Figure: Yield Distribution for the heavier masses of ^{235}U fission

INSTITUT FÜR CHEMIE (1): NUKLEARCHEMIE
KERNFORSCHUNGSANLAGE JÜLICH

1. Neutron Data

1.1 Nuclear Data Measurements on FR-Wall and Structural Materials

S.M. Qaim

(Relevant to request numbers: 682008, 691069, 691071, 691073, 691101, 692067, 692072, 692075, 692088 692105, 692107, 692111, 692308, 693312, 712011, 712012, 712016, 712025, 712026, 732042, 742034, 742048, 912008, 912009)

Activation cross sections at $E_n = 14.7 \pm 0.3$ MeV were determined using highly enriched isotopes, selective radiochemical separations and high-resolution Ge(Li) detector γ-ray spectroscopy with overall errors of about 10 % for (n,2n), (n,p) and (n,α) reactions (1) on nuclides of potential FR-wall and structural materials like Fe, Ni, Cr, Ti, W etc. Measurement of some (n,p) cross sections was also carried out in the region of rare earths.

The study of (n,n'p) and n,n'α) reactions initiated last year was continued further. Extensive use was made of radiochemical separations. The cross sections of these reactions are of the same order (2) as those for the corresponding (n,p) and (n,α) reactions. The contribution of these reactions should therefore also be taken into account while calculating the radiation demage to the first wall materials.

1.2 Investigation of (n,t) and (n,^{3}He) Reactions

S.M. Qaim, R. Wölfle, G. Stöcklin

In continuation of earlier radiochemical studies on fast-neutron induced trinucleon emission reactions, cross sections were measured at $E_n = 14.6 \pm 0.4$ MeV on ^{79}Br, ^{113}In, ^{127}I, ^{185}Re etc. In the case of (n,t) reactions an isotope effect was observed (3). The cross section ratio can be represented as

$$\frac{\sigma(n,t)_{Z,A+2}}{\sigma(n,t)_{Z,A}} = \exp 1.9 \left[(aE_m)^{1/2}_{A+2} - (aE_m)^{1/2}_{A}\right]$$

where a is the level density parameter and $E_m = E_n + Q - \delta$.

The (n,t) cross sections have also been measured at E_n = 22.5 MeV (53 MeV deuteron break-up neutrons) for the lightest nuclei like $^{6,7}Li$, ^{9}Be, ^{12}C, ^{16}O etc. using vacuum extraction of tritium followed by gas phase β^--counting. These lie in the mb region.

1.3 Evaluation, Compilation and Systematics of Fast Neutron Induced Data

S.M. Qaim, R. Wölfle, G. Stöcklin

Statistical model calculations using the Hauser-Feshbach method were carried out in collaboration with IKP (Jülich) and MPI (Heidelberg) for several target nuclides with A = 32 to 45. The results show that the (n,n'γ), (n,p), (n,α) and (n,t) reactions at 14.6 MeV proceed mainly via compound nucleus formation; the mechanism of the (n,^{3}He) reactions, however, is difficult to interpret.

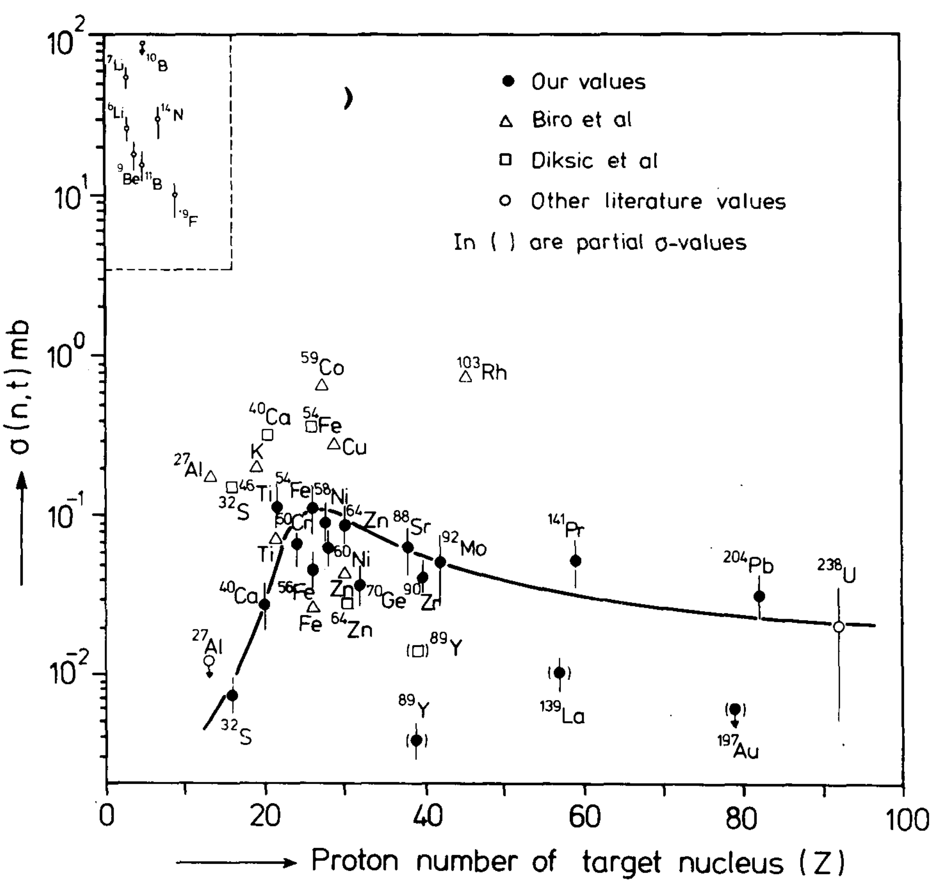

Fig. 1: Systematics of (n,t) reaction cross sections at 14 - 15 MeV

A survey of the fast neutron induced cross section data ($E_n \geq 14$ MeV) was performed and systematic trends in the data for (n,n'γ), (n,2n), (n,p) and (n,α) reactions were described (4). A critical appraisal of the nuclear data needs for fusion reactor design applications were carried out (5).

The systematics of (n,t) and (n,^{3}He) reaction cross sections were investigated in detail. The trends in the (n,t) cross sections at 14 MeV are shown (3) in Fig. 1. For medium and heavy mass nuclei both the (n,t) and (n,^{3}He) reaction cross sections decrease as a function of the relative neutron excess of the target nucleus. For elements with $Z > 22$ the (n,t) cross section at 14 MeV appears to be related to the neutron absorption cross section and can be described (3) by the empirical relation:

$$\sigma(n,t) = 4.52\ (A^{1/3} + 1)^2 \cdot \exp[-10\ (N-Z)/A]\ \text{in}\ \mu b.$$

At 22.5 MeV the (n,t) cross sections in the region of light nuclei decrease very sharply with the increasing atomic number of the target nucleus; in the region of medium and heavy mass nuclei they are, however, relatively independent of Z.

1.4 Measurement of Neutron Capture Cross Sections

H. Michael, A. Neubert, R. Wagner, A.J. Blair

Thermal neutron capture cross section and resonance integral of ^{138}La were determined by mass spectrometry (6) in combination with a Knudsen cell. Prior to irradiation a high enrichment (> 75 %) of ^{138}La, which is present in natural lanthanum only to the extent of 0.09 %, was carried out in the Jülich isotope separator SIDONIE II. The values obtained were

$$\sigma_o = 57.2 \pm 5.7\ \text{barn};\ I' = 384 \pm 90\ \text{barn}$$

2. Charged Particle Data

R. Weinreich, S.M. Qaim, G. Stöcklin

For optimizing the conditions of production of medically important radioisotopes, in continuation of our earlier studies excitation functions of several high-energy nuclear reactions were determined (7,8).

Thus, for the production of ^{28}Mg data were obtained in collaboration with IKP (Jülich) for the reactions $^{26}Mg(\alpha,2p)^{28}Mg$ and $^{27}Al(\alpha,3p)^{28}Mg$ as well as for the competing reactions $^{26}Mg(\alpha,p)^{29}Al$, $^{27}Al(\alpha,2p)^{29}Al$, $^{27}Al(\alpha,2pn)^{28}Al$, $^{27}Al(\alpha,3pn)^{27}Mg$, $^{27}Al(\alpha,4p3n)^{24}Na$, $^{27}Al(\alpha,4p5n)^{22}Na$ and $^{27}Al(\alpha,{}^{7}Be)^{24}Na$ over the α-energy range up to 160 MeV. Similarly for a comparative study of the production of ^{123}I via proton, deuteron and α-particle induced reactions, investigation of the excitation functions of the α-particle induced reactions of ^{127}I was started.

References

(1) S.M. Qaim, C. Graca, Nucl. Phys. A242 (1975) 317

(2) S.M. Qaim, R. Wölfle, G. Stöcklin, J. Radioanalyt. Chem., in press

(3) S.M. Qaim, G. Stöcklin, Nucl. Phys., in press

(4) S.M. Qaim, Nuclear Cross Sections and Technology, Vol. II, NBS special publication 425 (1975) 664

(5) S.M. Qaim, R. Wölfle, G. Stöcklin, Proc. Symposium on Fast-Neutron Interactions and on the Problems of High Current Neutron Generators, Debrecen, Hungary (August 1975) in press

(6) H. Michael, A. Neubert, R. Wagner, A.J. Blair, Int. J. appl. Radiat. Isotopes, in press

(7) R. Weinreich, W. Bräutigam, H.-J. Machulla, H.J. Probst, S.M. Qaim, G. Stöcklin, Experientia Suppl. 24 (1975) 457

(8) H.J. Probst, S.M. Qaim, R. Weinreich, Int. J. appl. Radiat. Isotopes, in press

I. INSTITUT FÜR EXPERIMENTALPHYSIK
UNIVERSITÄT HAMBURG

Excitation Function of the Reaction $^{232}Th(n,2n)^{231}Th$ in the Energy Region E_n = 13 - 18 MeV

H. Karius, M. Bormann[+], W. Scobel
(Related to request number: 671083)

This work continues our studies (1) of (n,2n) reactions in the actinide region. Attention has been focussed on the depletion of compound contributions due to precompound decay modes.

The reaction $^{232}(n,2n)^{231}$Th has been studied with the activation technique using a Ge(Li) diode with high energy resolution to detect the 84.2 keV γ activity of $^{231}Pa^{+}$ following the 25.6 h ß-activity of ^{231}Th. Special attention has been paid to a careful separation of the γ line of interest from γ transitions coming from spontaneous decay of ^{232}Th and its daughters.

The experimental cross sections are listed in Table 1. The analysis similar to that (1) for ^{238}U shows, that above the (n,3n) threshold at 11.6 MeV the (n,2n) excitation function substantially exceeds the predictions of the statistical model. These contributions are due to emission of a first neutron during the equilibration and are properly described by the geometry dependent hybrid model (2).

Table 1: Cross Sections of $^{232}Th(n,2n)^{231}Th$

E_n (MeV) Energy (MeV)	σ(n,2n) (mb) σ (barn)	E_n (MeV) Energy (MeV)	σ(n,2n) (mb) σ (barn)
12.99 ± .11	1811.2 ± 246	15.85 ± .14	552.3 ± 53
13.83 ± .04	1565.9 ± 148	16.57 ± .16	437.7 ± 42
14.31 ± .08	1234.6 ± 118	17.28 ± .18	368.9 ± 34
14.79 ± .19	1048.6 ± 99	18.13 ± .21	303.1 ± 27
15.32 ± .17	792.3 ± 108		

References

(1) A. Ackermann, B. Anders, M. Bormann, W. Scobel, Proceedings Conf. on Nuclear Cross Sections and Technology (Washington 1975) p. 819

(2) M. Blann, Nucl. Phys. A213 (1973) 570

+Present address: Ruhr Universität Bochum, Abt. für Physik und Astronomie

INSTITUT FÜR KERNCHEMIE
JOHANNES GUTENBERG-UNIVERSITÄT MAINZ

1. Charge Distribution in Thermal Neutron Induced Fission Reactions

H.O. Denschlag, G. Fischbach, H. Meixler, G. Paffrath, W. Rudolph, M. Weis

(Related to request numbers: 671105, 671107, 711802, 671125, 671126, 671128, 711803)

The study of charge distribution in nuclear fission besides its basic interest which consists in providing information on the nuclear temperature at the scission configuration (polarization of nuclear matter, shell- and pairing effects) has some very partical importance for the calculation of after-heat in an emergency shut down of a nuclear reactor.

Table I shows a number of fractional independent and/or cumulative yields which have been measured recently at Mainz by radiochemical methods. The values are taken from unpublished and unfinished experimental studies and should therefore be quoted only with written permission of the authors.

Table I

Fractional yields of some fission products

fission reaction	fission product	fractional yield % independent	fractional yield % cumulative	origin
$^{235}U(n_{th},f)$	^{99}Y		31,4 ± 3,9	a
	^{99}Zr	56,9 ± 4,3	88,3 ± 2,8	a
	$^{99}Nb^{m}$	11,7 ± 2,8	36,4 ± 4,5	a
	$^{99}Nb^{g}$	< 1	63,6 ± 4,5	a
	^{99}Nb(sum)	11,7 ± 2,8	100,0	a
	$^{132}Sb(8^-/4^+)$	0,42 ± 0,03(IR)		b,c
	^{134}Sb(10 s)		6,15 ± 0,40	c
	^{134}Sb(0,8 s)		1,23 ± 0,08	c
	^{135}Sb		2,3 ± 0,1	c
	^{146}La		80 ± 4	e
	^{146}Ce		98 ± 2	e
$^{239}Pu(n_{th},f)$	^{131}Sn		12 ± 3	b
	^{132}Sn		9,0 ± 1,7	b
	$^{132}Sb(8^-/4^+)$	0,33 ± 0,05(IR)		b
	$^{132}Sb(8^-)$	16,6 ± 3,3		b
	$^{132}Sb(4^+)$	33,8 ± 4,2		b
	^{132}Sb(sum)	50,4 ± 2,5		b
	^{132}Te	39,6 ± 1,2		b
	^{133}Sb		32 ± 4	b
	^{134}Sb(10 s)		3,8 ± 1,0	b
	^{134}Sb(10 s)		3,2 ± 0,7	c
	^{135}Sb		0,73 ± 0,16	c

-2-

Table I continued

Fractional yields of some fission products

fission reaction	fission product	fractional yield % independent	cumulative	origin
$^{249}Cf(n_{th},f)$	^{132}Sn		< 3	b
	$^{132}Sb(8^-/4^+)$	0,47 ± 0,05(IR)		b
	$^{132}Sb(8^-)$	16 ± 6		b
	$^{132}Sb(4^+)$	18 ± 7		b
	$^{132}Sb(sum)$	35 ± 10		b
	^{139}Xe		32 ± 5	d

(IR) indicates the yield ratio of two isomeric states. This value is shown when it was measured directly.

a) M. Weis, doctoral thesis, Univ. of Mainz, in preparation
to be published in J. inorg. nucl. Chem.

b) G. Paffrath, doctoral thesis, Univ. of Mainz, in preparation,
to be published

c) W. Rudolph " " "

d) H. Meixler " " "

e) G. Fischbach " " "

2. Delayed-Neutron Spectra Following Decay of ^{85}As, ^{87}Br, ^{135}Sb and ^{137}I

W. Rudolph, H. Ohm and K.-L. Kratz

(Relevant to request numbers: 691259, 691260, 712061)

In contrast to predictions from theory (1,2) a great number of delayed-neutron spectra exhibit discrete structure.

We have investigated the delayed-neutron emission of two nuclides with a small energy window ($Q_{\beta}-B_n$) for neutron emission; e.g. ^{87}Br and ^{137}I, and of two nuclei with a large energy window; e.g. ^{85}As and ^{135}Sb (3,4). These nuclides were obtained from thermal-neutron-induced fission of ^{235}U by fast radiochemical separations based on isotope exchange (5) and hydride volatilization (6), respectively. The delayed-neutron spectra are shown in Figs. 1-4. A dominant feature of these spectra is the prominent line structure with densities small compared to the expected level densities (e.g., the number of neutron lines for ^{85}As decay account for about 1 % of the levels available through allowed β decay (7)). The energies and intensities of the strongest neutron lines given in Table 1 and 2 were obtained by computer analysis (8,9). In all four cases the line structure accounts for the majority ($\geq$ 60 %) of the total neutron intensity of each spectrum.

A second feature of ^{85}As and ^{135}Sb delayed-neutron spectra is the absence of appreciable neutron intensity above 1.6 MeV (^{85}As) and 2.0 MeV (^{135}Sb) even though ranges of 5.0 MeV and 3.6 MeV are possible for the neutron energies. Through gamma ray studies we have been able to demonstrate that this effect is due to the dominance of neutron emission from intermediate levels to excited states in the final nuclides (3,10).

We conclude from the experimental data that the line structure in delayed-neutron spectra is due to selectivity in β decay and in the subsequent neutron emission to levels in the final nucleus.

References

(1) A.C. Pappas and T. Sverdrup, Nucl. Phys. A188 (1972) 48

(2) K. Takahashi, Progr. Theor. Phys. 47 (1972) 1500

(3) H. Franz et al., Phys. Rev. Lett. 33 (1974) 859

(4) H. Ohm, Diplomarbeit, Universität Mainz (1975) and unpublished results

(5) W. Eckhardt et al., Z. Anal. Chem. 226 (1967) 71

(6) H. Folger et al., Radiochem. Radioanal. Lett. 1 (1969) 185

(7) A. Gilbert and A.G.W. Cameron, Can. J. Phys. 43 (1965) 1446

(8) J.T. Routti and S.G. Prussin, Nucl. Instr. Methods 72 (1969) 125

(9) Program Library, Institut für Kernchemie Mainz (1975)

(10) W. Rudolph, Doctoral Dissertation, Mainz (1976), to be published

Table 1

Energies (keV) and relative intensities of neutron lines from the decay of ^{85}As and ^{87}Br

^{85}As				^{87}Br			
E_n	(ΔE_n)	I_n	(ΔI_n)	E_n	(ΔE_n)	I_n	(ΔI_n)
55,9	(1,2)	16	(3)	18,2	(0,7)	100	(3)
96,2	(1,6)	26	(5)	40,7	(1,1)	16	(2)
139,8	(3,3)	11	(5)	52,3	(0,7)	75	(3)
171,2	(1,4)	46	(8)	70,8	(1,4)	37	(7)
210,0	(6,5)	5	(2)	80,3	(2,1)	24	(8)
245,0	(6,4)	5	(2)	120,5	(1,0)	32	(3)
270,9	(2,1)	15	(7)	136,0	(1,9)	36	(10)
314,5	(3,1)	17	(5)	147,5	(1,8)	31	(6)
343,6	(2,7)	21	(6)	169,2	(2,4)	10	(3)
426,2	(3,9)	16	(5)	181,8	(1,0)	46	(4)
494,4	(2,5)	100	(12)	211,2	(2,4)	9	(4)
515,7	(2,8)	87	(16)	248,0	(0,8)	69	(6)
565,2	(2,8)	62	(10)	256,3	(2,5)	15	(3)
640,0	(2,9)	96	(15)	312,4	(1,5)	13	(3)
707,9	(3,3)	51	(9)	339,3	(3,1)	5	(2)
925,2	(4,3)	73	(11)	386,1	(2,2)	8	(2)
1012,6	(4,6)	69	(12)	407,4	(1,5)	12	(2)
1154,0	(6,7)	36	(11)	437,7	(1,1)	20	(2)
1186,9	(7,6)	34	(10)	457,0	(1,8)	10	(2)
1419,6	(6,6)	40	(7)				
1506,4	(9,7)	20	(3)				

Table 2

Energies (keV) and relative intensities of neutron lines from the decay of ^{135}Sb and ^{137}I

^{135}Sb				^{137}I			
E_n	(ΔE_n)	I_n	(ΔI_n)	E_n	(ΔE_n)	I_n	(ΔI_n)
162,6	(1,8)	14	(4)	77,2	(0,7)	28	(6)
355,5	(2,2)	13	(4)	154,2	(1,5)	8	(2)
496,4	(3,9)	11	(4)	255,2	(0,9)	27	(6)
546,3	(2,3)	15	(5)	268,5	(0,8)	33	(5)
591,1	(2,4)	11	(3)	318,7	(1,5)	23	(4)
618,2	(2,9)	12	(4)	347,1	(1,8)	10	(2)
733,3	(2,7)	13	(4)	371,6	(0,7)	100	(3)
788,3	(3,2)	13	(4)	389,9	(0,9)	33	(5)
815,0	(2,7)	25	(5)	414,6	(1,1)	26	(6)
843,1	(2,6)	22	(5)	455,6	(1,2)	13	(2)
972,4	(2,8)	27	(5)	476,2	(1,0)	51	(4)
1035,4	(2,3)	94	(10)	498.0	(1,2)	40	(6)
1193,3	(2,6)	53	(7)	514,3	(1,4)	26	(6)
1283,1	(3,8)	32	(6)	555,0	(1,2)	32	(5)
1318,8	(3,6)	32	(6)	577,1	(1,0)	48	(5)
1372,3	(4,1)	20	(6)	601,2	(1,4)	15	(2)
1449,2	(3,1)	100	(7)	682,3	(1,7)	8	(2)
1511,7	(4,0)	16	(5)	719,4	(1,7)	8	(2)
1608,0	(5,1)	9	(4)	741,7	(1,4)	31	(7)
1802,6	(5,5)	9	(5)	766,9	(1,6)	15	(2)
1897,3	(5,1)	33	(6)	837,6	(1,6)	13	(3)

Table 2 cont.

Energies (keV) and relative intensities of neutron lines from the decay of ^{135}Sb and ^{137}I

^{135}Sb				^{137}I			
E_n	(ΔE_n)	I_n	(ΔI_n)	E_n	(ΔE_n)	I_n	(ΔI_n)
				849,4	(1,3)	45	(7)
				946,3	(1,5)	23	(3)
				966,5	(1,8)	13	(3)
				992,6	(1,9)	9	(3)
				1047,4	(1,9)	11	(3)
				1125,0	(2,0)	11	(3)
				1146,4	(1,8)	26	(3)
				1175,5	(2,0)	11	(3)
				1196,6	(2,0)	10	(3)

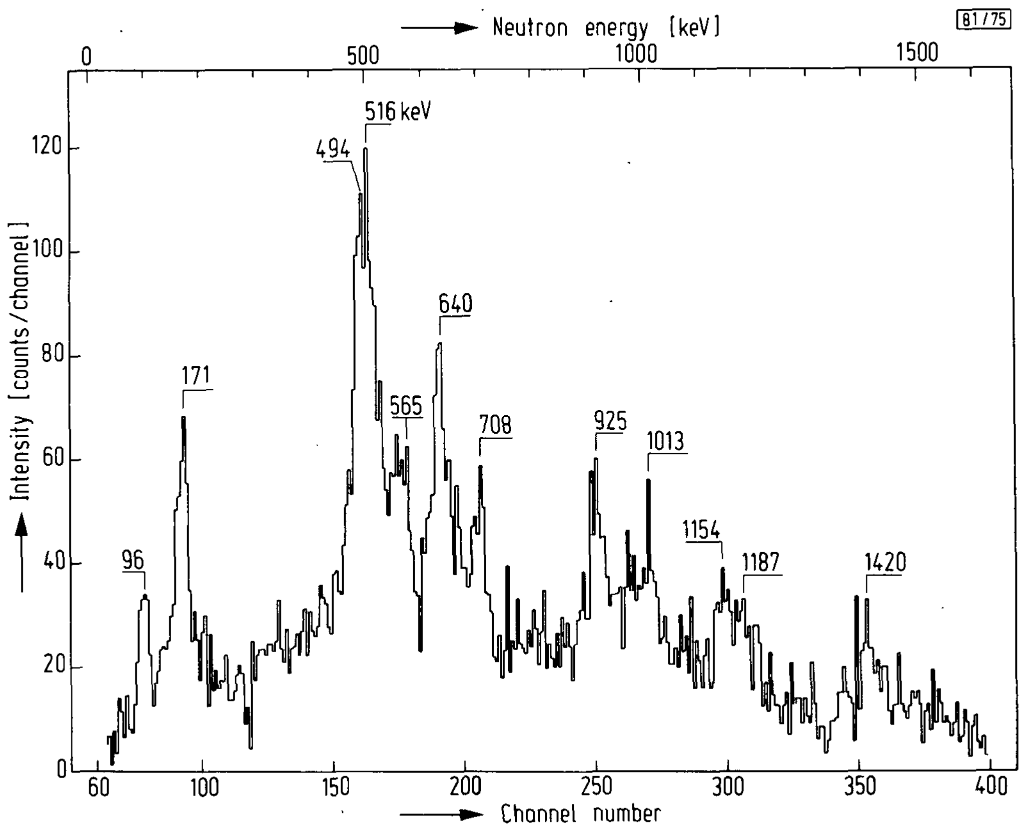

Fig. 1: Delayed-neutron spectrum following decay of 2.05 sec ^{85}As, corrected for relative detection efficiency snd detector response function.

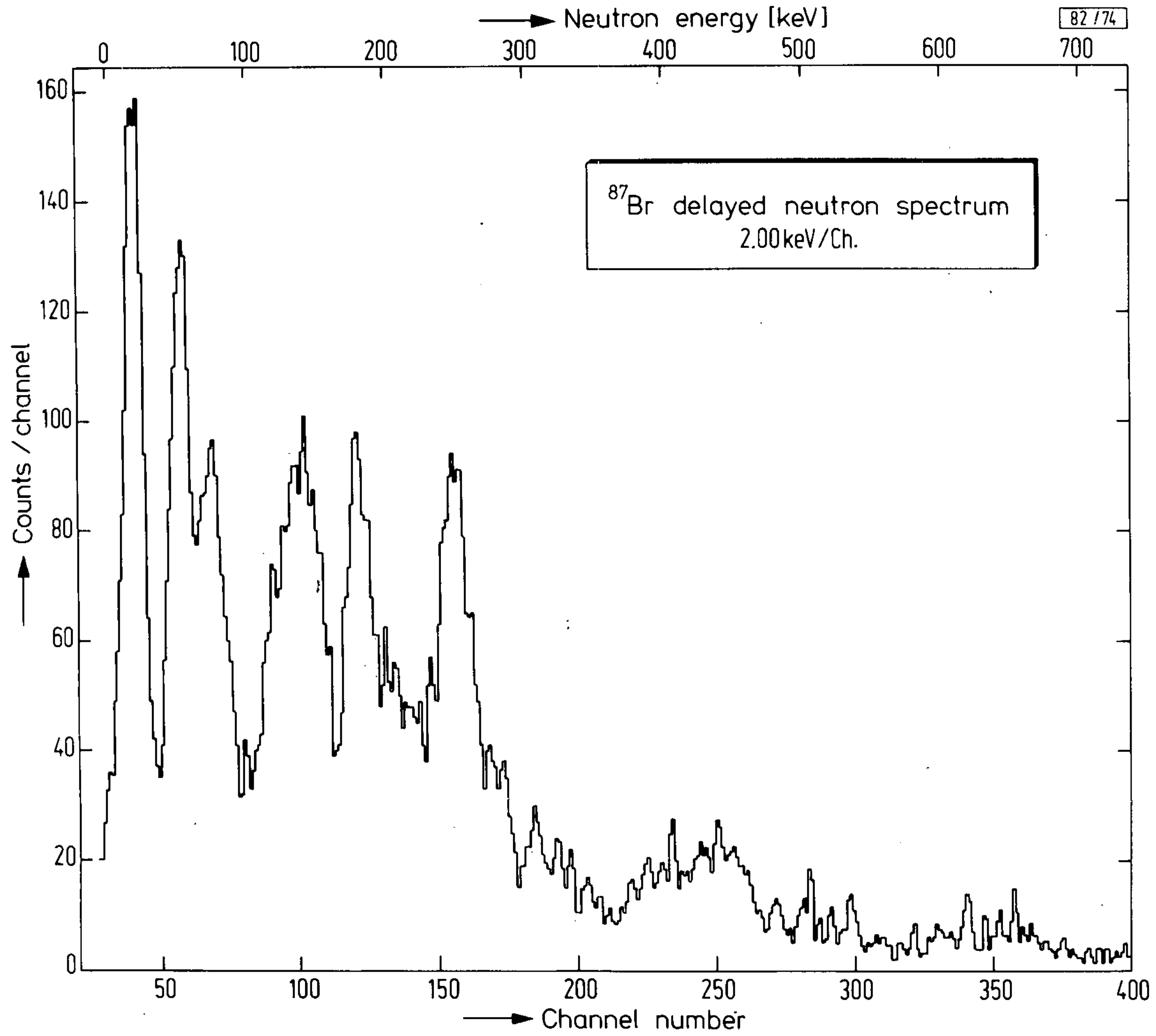

Fig. 2: Delayed-neutron spectrum following decay of 55 sec ^{87}Br, corrected for relative detection efficiency and detector response function.

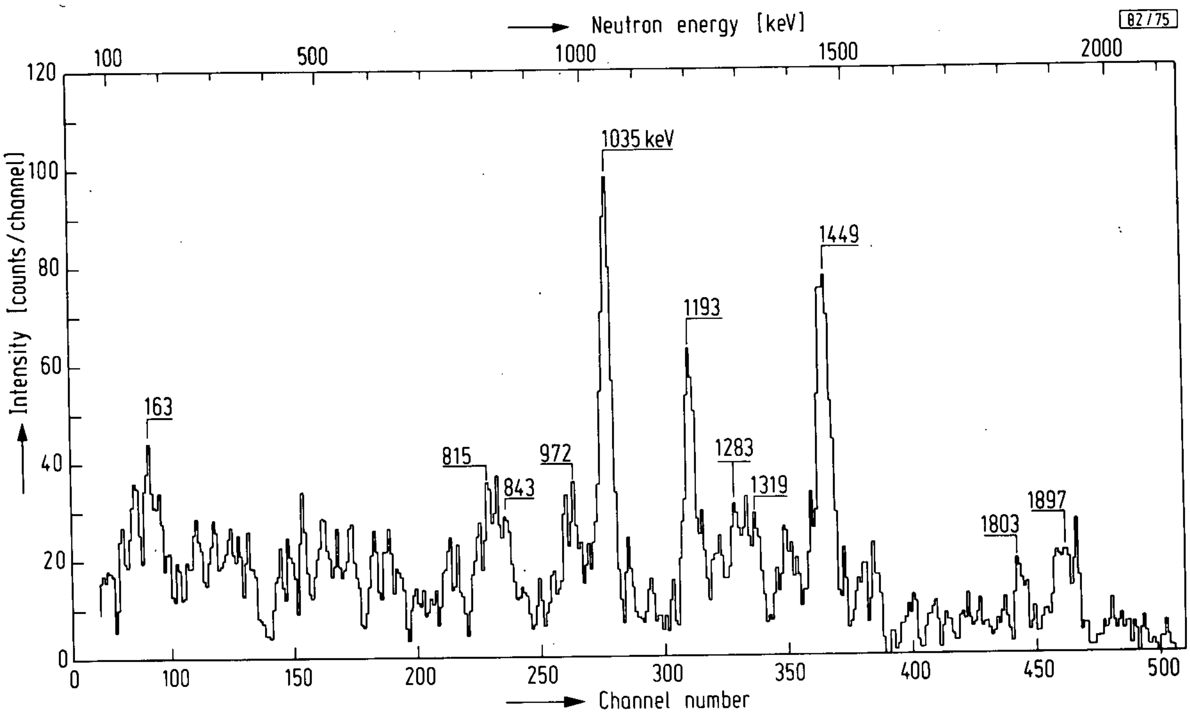

Fig. 3: Delayed-neutron spectrum following decay of 1.70 sec ^{135}Sb, corrected for relative detection efficiency and detector response function.

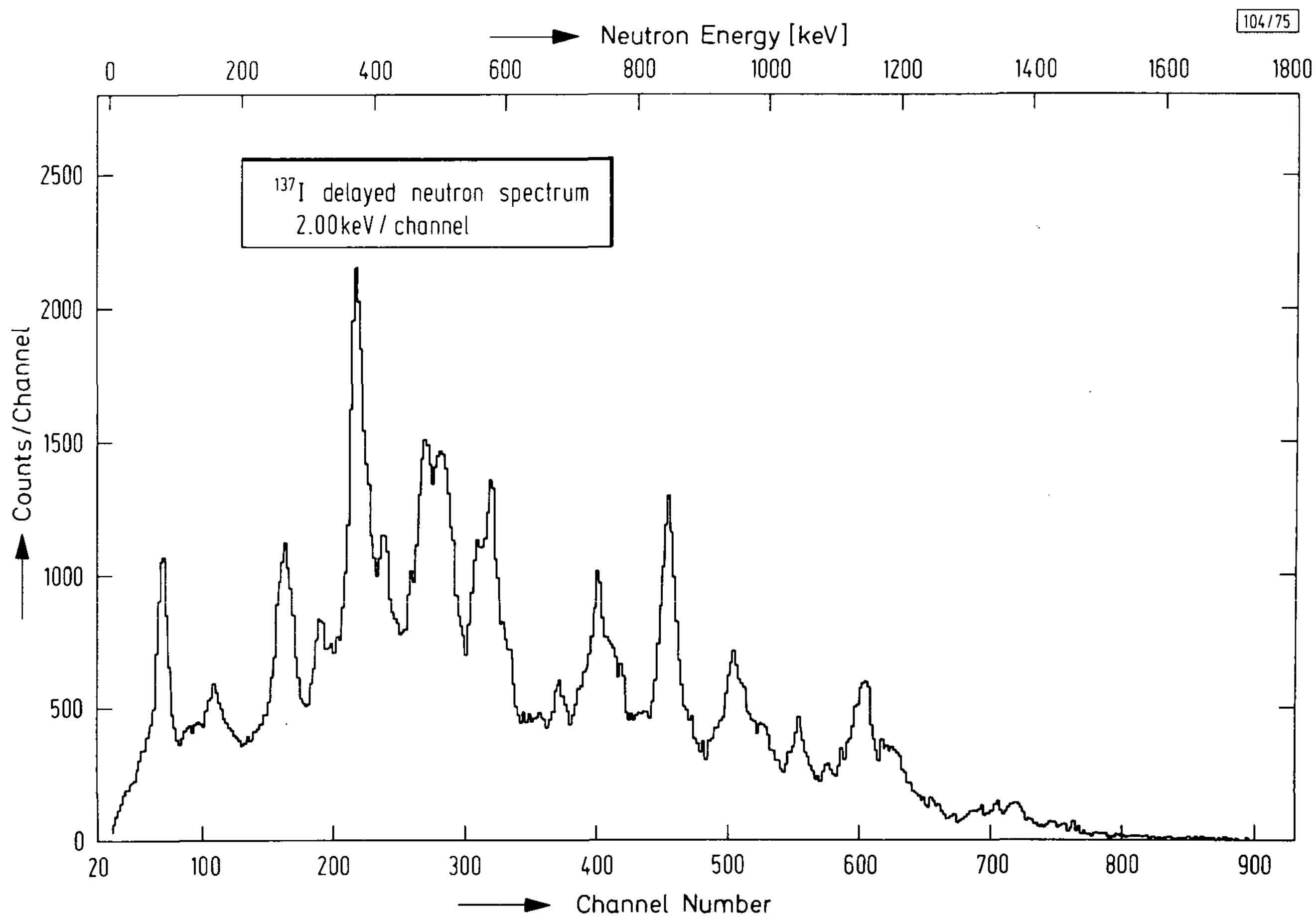

Fig. 4: Delayed-neutron spectrum following decay of 24 sec ^{137}I, corrected for relative detection efficiency and detector response function.

3. Decay Properties of Fission Products in the Mass Region A~100[§]

H. Ahrens[+], G. Franz[+], G. Herrmann, N. Kaffrell, G. Klein,
K. Summerer, G. Tittel, N. Trautmann

Neutron-rich nuclei in the mass region A~100 are predicted to form a new region of stable quadrupole deformation. Compared with the well-known deformed nuclei in the rare-earth region, however, nuclei around A~100 should be softer towards ß and γ deformations, as follows from the calculated potential energy surfaces of these nuclei.

From the experimental point of view, studies of neutron-rich nuclei in this region are hampered by the fact that the most interesting nuclei have rather short half-lives and that nuclear fission of heavy elements is the only way to produce them.

Our approach to get more insight into the properties of these nuclei consists in a combination of fast, automated chemical separations with high-resolution γ-ray spectroscopy. As a first step towards this goal, we have worked out separation techniques (1-5) for Y, Zr, Nb, Mo, Tc and Ru and applied these techniques to the identification of short-lived isotopes of these elements. In addition, more detailed spectroscopic investigations like γγ-coinicidence measurements have been performed in order to get the decay schemes of the most interesting nuclei. The activites have been produced by thermal-neutron induced fission of ^{235}U, ^{239}Pu and ^{249}Cf.

In some cases (Zr, Nb, Mo), where the mass assignments were ambiguous, additional measurements have been performed with mass-separated sources obtained with the fission product separator 'LOHENGRIN' in Grenoble. Here, only ^{235}U was available as fissile material.

The main results of our investigation are summarized in Table 1.

[§] Part of these results have been obtained in collaboration with J.P. Bocquet, E. Monnand, B. Pfeiffer and F. Schussler at the fission product separator 'LOHENGRIN' in Grenoble

[+] GSI, Darmstadt

References

(1) G. Klein, N. Kaffrell, N. Trautmann and G. Herrmann, Inorg. Nucl. Chem. Letters 11 (1975) 511

(2) N. Trautmann, N. Kaffrell, H.W. Behlich, H. Folger, G. Herrmann, D. Hübscher and H. Ahrens. Radiochim. Acta 18 (1972) 86

(3) H. Ahrens, N. Kaffrell, N. Trautmann and G. Herrmann, Phys. Rev. C (in press)

(4) N. Trautmann, N. Kaffrell, H. Ahrens and P.F. Dittner, Phys. Rev. C (in press)

(5) G. Franz and G. Herrmann, Inorg. Nucl. Chem. Lett. 11 (1975) 857

(6) K. Sümmerer, N. Kaffrell and N. Trautmann, Z. Phys. A273 (1975) 77

(7) N. Kaffrell, N. Trautmann, G. Herrmann and H. Ahrens, Phys. Rev. C8 (1973) 320

Table 1

Nuclide	Half-life	Strongest γ-rays [keV]	Ref.
Y-96	9.6±0.3 sec	617.7, 914.6, 1106,6, 1750.3;	(1)
Y-97	1.5±0.3 sec	161.4, 1102.9;	
	3.6±0.3 sec	1290.8, 1399.4, 3287.5, 3401.2;	
Zr-99	2.0±0.2 sec	387.6, 469.2, 546.2, 594.1;	
Zr-100	7.1±0.4 sec	401.0, 504.6;	
Zr-101	2.0±0.3 sec	-	(2)
Zr-102	2.9±0.2 sec	-	(3)
Nb-100	1.5±0.2 sec	159.3, 528.1, 535.4, 1022.1;	(3)
	3.1±0.3 sec	535.4, 600.2, 966.2, 1280.4;	(3)
Nb-101	7.1±0.3 sec	118.5, 157.7, 180.6, 276.2;	(3)
Nb-102	1.3±0.2 sec	296.0, 400.6, 551.6, 847,6;	(3)
	4.3±0.4 sec	296.0, 447.0, 1235.4, 1632.7;	(3)
Nb-103	1.5±0.2 sec	102.7, 126.5, 241.5, 247.7;	
Nb-104	0.8±0.2 sec	192.2, 386.5, 477.4, 812.5;	
	4.8±0.4 sec	192.2;	(3)
Nb-105	2.8±0.3 sec	94.3, 246.7, 310.0;	
Nb-106	~1 sec	171.7;	(3)
Mo-103	68.0±1.0 sec	45.8, 83.4, 150.2, 424.0;	
Mo-104	60.0±2.0 sec	68.6, 91.0, 375.8, 420.8;	
Mo-105	36.0±2.0 sec	64.2, 85.6, 147.8, 249.5;	
Mo-106	8.2±1.0 sec	53.9, 465.7, 595.3, 618.6;	
Mo-107	3.5±0.5 sec	64.4, 400.1, 483.3;	
Tc-103	54.2±0.8 sec	136.1, 210.2, 346.3, 562.8;	
Tc-104	18.5±0.5 min	357.8, 530.6, 535.2, 562.8;	
Tc-105	7.6±0.1 min	108.0, 143.2, 159.3, 321.5;	(6)
Tc-106	36.0±1.0 sec	270.3, 522.4, 720.8, 792,7;	(7)
Tc-107	21.0±1.0 sec	102.7, 106.3, 177.2, 458.9;	(2)
Tc-108	5.0±0.2 sec	242.4, 465.8, 708.1, 732.4;	(7)
Tc-109	1.4±0.4 sec	-	(4)
Tc-110	1.0±0.2 sec	240.8;	(4)

Table 1 (continued)

Nuclide	Half-life	Strongest γ-rays [keV]	Ref.
Ru-107	3.8±0.1 min	194.1, 374.5, 462.7, 847.8;	(5)
Ru-108	4.6±0.1 min	165.1;	(5)
Ru-109	34.5±1.0 sec	206.2, 225.9, 358.7, 1928.9;	(5)
	12.9±1.0 sec	-	(5)
Ru-110	12.6±0.5 sec	95.8, 112.1;	(5)
Ru-111	3 ± 1 sec	-	(5)
Ru-112	3.6±0.5 sec	-	(5)
Ru-113	3.0±0.7 sec	303.6;	(5)
Rh-108	17 ± 1 sec	434.1, 497.1, 618.9;	(5)
Rh-109	79.8±1.0 sec	178.0, 291.4, 326.7, 426.1;	(5)
Rh-110	3.3±0.3 sec	373.7, 439.7;	(5)
Rh-111	11 ± 1 sec	275.3;	(5)
Rh-112	<1.5 sec	348.6;	(5)

INSTITUT FÜR REINE UND ANGEWANDTE KERNPHYSIK
UNIVERSITÄT KIEL, GEESTHACHT

Fast-Chopper Time-of-Flight Spectrometer

H.G. Priesmeyer, U. Harz, K. Freitag

1. Gross Fission Product Measurements and Isotopic Content Determinations

Measurements of GFP samples have been extended down to 0.2 eV. The transmission of low enrichment nuclear fuel (from the KWO power plant) shows the resonances of breeded ^{239}Pu at 0.296 eV and ^{240}Pu at 1.056 eV, which may be used for content determination.

Fig. 1 shows the transmission of the KWO sample in the low energy range.

A resonance at 2.67 eV can be assigned to ^{242}Pu. A significant difference appears between the transmissions of irradiated high enrichment and low enrichment fuel on both wings of the 8.0 eV ^{152}Sm resonance, as can be seen in Fig. 2. The resonance at 7.69 eV is possibly due to a transuranium isotope, probably ^{244}Cm. Cooling of the sample will be necessary to reduce the Doppler width and improve the structure of the resonances.

A sample for nondestructive content determination of fissile and fission product materials has been prepared.

2. Measurements of Cd-Isotopes

The measurements on the isotopes $^{106,108}Cd$ and ^{114}Cd are made in partial fulfilment of WRENDA request 752002. The experiments on ^{114}Cd (enriched to 40.5 %) are completed, resonance analysis is being done. The measurements on ^{106}Cd (enrichment 88.4 %, 2.4 g of CdO, on loan from US ERDA) have been begun. There seems to be no resonance below 100 eV in this isotope.

3. Fission-Product Cs Mixture

An experiment with a second $^{133,35,37}Cs$ sample of about five times the thickness of the first sample has been prepared in order to get better values for the parameters of the two resonances so far discovered below 1 keV. Special care will have to be taken on the assignment of the 880 eV resonance.

The measurements contribute to several WRENDA requests.

4. Publications

Atomkernenergie 25 (1975), 109 and GKSS 75/E/17

NBS Special Publication 425, p. 744 ff.

IAEA-SM 201/4

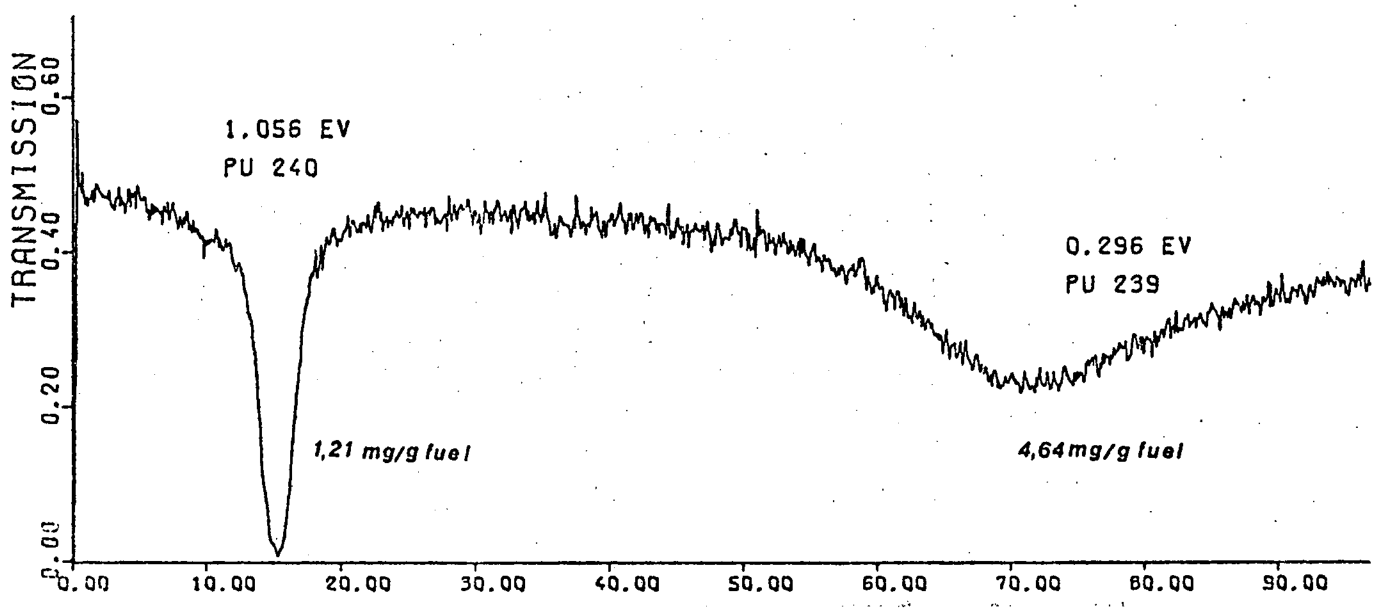

Fig. 1: Low-energy transmission of gross fission product sample from KWO fuel rod (2.8 % original ^{235}U enrichment)

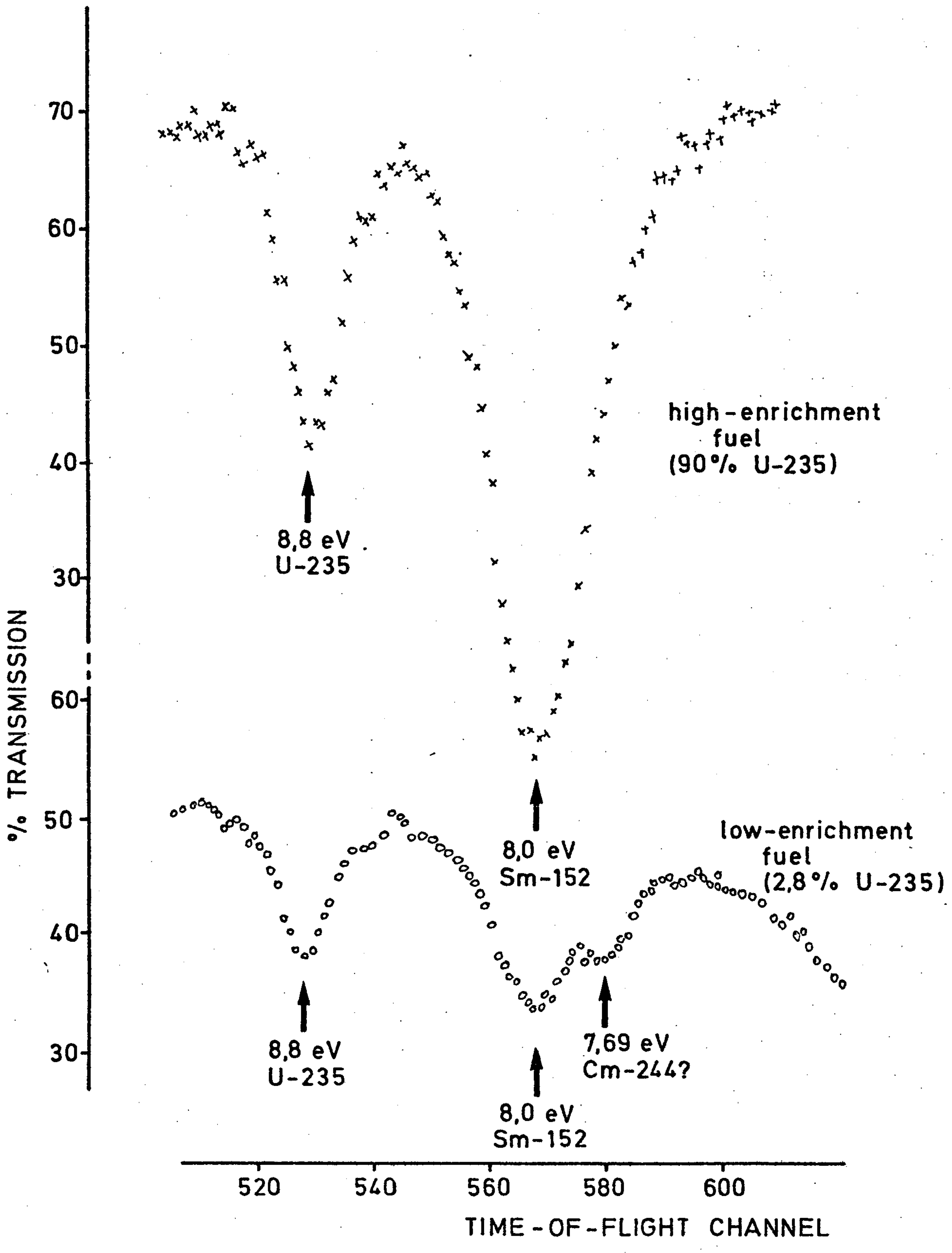

Fig. 2: Comparison of gross fission transmissions near 8 eV

PHYSIK-DEPARTMENT DER TECHNISCHEN UNIVERSITÄT MÜNCHEN
FORSCHUNGSREAKTOR FRM, GARCHING

Nuclear Structure Study with Slow Neutrons

1. Measurement of the Neutron-Electron Interaction by the Scattering of Neutrons by Lead and Bismuth+

L. Koester, W. Nistler*, and W. Waschkowski

We report on precision experiments for the measurement of the atomic coherent scattering length of lead and for the measurements of the neutron total cross sections of lead and bismuth from which we could derive the nuclear scattering lengths. The experiments yielded the following results:

b_c (Pb-atom) = 9.4003 ± 0.0014 fm
b_N (Pb-nucleus) = 9.5121 ± 0.0015 fm and
b_N (Bi-nucleus) = 8.6412 ± 0.0015 fm

From these data and with the previously reported b_c(Bi-atom) we obtain two new values for the neutron-electron scattering length

$b_{ne} = -1.364 \pm 0.025 \cdot 10^{-3}$ fm from the Pb-experiment and
$b_{ne} = -1.393 \pm 0.025 \cdot 10^{-3}$ fm from the Bi-data

The mean value $b_{ne} = -1.378 \pm 0.018 \cdot 10^{-3}$ fm differs from the Foldy term but agrees with the average of previous values.

+ Abstract of a paper to be published
* Present address: Physikalisch-Technische Bundesanstalt
D-3300 Braunschweig, Germany

2. Exact Determination of Free Cross Sections for Neutrons+

W. Waschkowski and L. Koester

We investigated the application of rotating activation foils of resonance energies 1.26 and 5.19 eV for exact measurements of neutron cross section. The detector consisting of a sandwich of two rotating foils was suitable for measuring exactly the neutron flux at the resonance energy and for detecting energy changes in the neutron beam. By means of experiments on solid and liquid samples we found in the cross sections of polycrystalline samples uncertainties greater than the statiscal error.

The more accurate measurements on liquid samples yielded values of the free scattering cross sections adjusted at zero energy as follows:

Lead: $\sigma_o(Pb) = 11.261 \pm 0.006$ b;
Bismuth: $\sigma_o(Bi) = 9.300 \pm 0.003$ b and
Sulfur: $\sigma_o(S) = 0.985 \pm 0.004$ b.

These data are of interest for an investigation of the neutron-electron interaction.

+ Abstract of a paper to be published in Naturforschung.

3. The Scattering of Slow Neutrons by Phosphorus and Nitrogen+

L. Koester, K. Knopf, and W. Waschkowski

The coherent scattering lengths b and the free cross sections for the scattering of slow neutrons by P and N were measured on powdered samples. From the results we derived data for the incoherent cross sections and for the spin state scattering lengths.

We found for phosphorus:

$b = 5.13 \pm 0.01$ fm, $\sigma_{free} = 3.134 \pm 0.010$ b and $\sigma_{inc} = 0.006 \pm 0.016$ b,

and for nitrogen:

$b = 9.36 \pm 0.02$ fm, $\sigma_{free} = 10.03 \pm 0.08$ b and $\sigma_{inc} = 0.4 \pm 0.1$ b.

Derived values for resonance parameters of N are given.

+ Abstract of a paper to be published in Z. f. Physik

4. Determination of Scattering Amplitudes and Scattering Cross Sections

L. Koester, K. Knopf, and W. Waschkowski

By transmission experiments scattering cross sections at neutron energies of 1.26 eV and 5.2 eV are measured with resonance activation detectors in a device described in abstract 2. We used metallic samples of Mg, Be, Ni, Cr, Al, Nb, V, Zn and Ge in powdered and solid form. On chemical compounds BaF_2, BaCl, $BaCO_3$, $BaSO_4$ and $Ba(NO_3)_2$, partly we could take single crystals, we determined the scattering cross section on Ca, Sr, Ba, and Na and Cl.

By means of Christiansenfilter technique the coherent atomic scattering length of the compounds were measured. A possible water contamination could be detected down to relative weight concentration of 10^{-4} by using transmission measurements at a neutron wavelength of 12 Å.

Measurements continue

From both values, the scattering amplitude and the scattering cross section, the incoherence cross section could be calculated for the mentioned substances.

ZENTRALSTELLE FÜR ATOMKERNENERGIE-DOKUMENTATION (ZAED)

1. An Information System for Physics Data in the Federal Republic of Germany

H. Behrens and G. Ebel

The Zentralstelle für Atomkernenergie-Dokumentation (ZAED) located at the Karlsruhe Nuclear Research Center has been commissioned by the German Federal Ministry for Science and Technology to establish an information system for physical data. For this purpose data compilations will be provided for a number of subfields of physics which will be updated regularly.

The data information system consists i) of a number of groups compiling the data and ii) of a central office for coordination and management.

i) The data themselves are collected and, if necessary, evaluated by decentralized groups of specialists working at research institutions. These groups are actively engaged in the same field in which they compile data. In addition they are responsible for updating their compilations over a longer period of time. Data from all fields of physics (nuclear physics included) are entered into the data information system. The data can be of experimental or theoretical type and may be represented in the form of tables, curves or parametrized formulae.

ii) The central office of the data information system is located at the ZAED and will provide the following services:

1. Technical support to the compiling groups such as providing references to the relevant primary literature by means of magnetic tape services.
2. To a certain extent, financial support to the compiling groups, covering expenses and a honorarium.
3. Editing, publishing and distribution of the data compilations.
4. Computer processing of the data and preparation of data tapes.
5. Coordination of the compiling activities of the different groups, organization and management of the whole data information system.

The data compilations are published as individual booklets within a series called "Physikdaten/Physics Data" under the authorship of the compilers. The explanatory text of the compilations is in English or in English and German. This form of single pamphlets has the advantage of being allways at hand and of easy replacement of older editions by updated revisions. The compilations are distributed to research institutes, industrial laboratories, libraries and individual scientists.

The first issue with the title "Survey Index of Pion-Nucleon Scattering Data" has already been published.

Further topics in the field of nuclear physics will include:
curves of neutron cross sections, total internal conversion coefficients; beta decay data; fluorescence yields etc..

Future plans envisage a bibliography of charged particle total cross section data in cooperation with the IAEA. A further intention is to participate in the compilation and evaluation of nuclear structure data in cooperation with Brookhaven, USA, IAEA, Vienna, and institutions of other countries.

In addition to the preparation of new data compilations an index of already existing compilations will be set up. Such an index of data compilations will be published in booklet form and maintained as a computerstored file that will allow rapid access to data compilations with regard to a specific requirement.

Addresses of Contributing Laboratories

Institut für Angewandte Kernphysik II
Director: Prof. Dr. G. Schatz
Kernforschungszentrum Karlsruhe
Postfach 3640
7500 Karlsruhe

Institut für Neutronenphysik und Reaktortechnik
Director: Prof. Dr. K. Wirtz
Kernforschungszentrum Karlsruhe
Postfach 3640
7500 Karlsruhe

Institut für Radiochemie
Director: Prof. Dr. Seelmann-Eggebert
Kernforschungszentrum Karlsruhe
Postfach 3640
7500 Karlsruhe

European Institute for Transuranium Elements
Director: Prof. Dr. Lindner
Euratom Karlsruhe
Postfach 2266
7500 Karlsruhe

Institut für Chemie (1) : Nuklearchemie
Director: Prof. Dr. G. Stöcklin
Kernforschungsanlage Jülich
Postfach 1913
5170 Jülich 1

I. Institut für Experimentalphysik
Director: Prof. Dr. H. Neuert
Universität Hamburg
Luruper Chaussee 149
2000 Hamburg 50

Institut für Kernchemie
Director: Prof. Dr. G. Herrmann
Johannes Gutenberg-Universität Mainz
Friedrich-von-Pfeiffer-Weg 14
6500 Mainz

Institut für Reine und Angewandte Kernphysik
Director: Prof. Dr. G. Wibberenz
Universität Kiel, Geesthacht
Reaktorstr. 1
2054 Geesthacht/Tesperhude

Physik-Department der Technischen Universität München
Abteilung E14, Forschungsreaktor
Director: Dr. L. Köster
8046 Garching/München

Zentralstelle für Atomkernenergie-Dokumentation (ZAED)
Director: Dr. W. Rittberger
Kernforschungszentrum
7514 Eggenstein-Leopoldshafen 2